THE UNIVERSITY OF READING

A DYNAMICAL APPROACH STUDY OF SOME EXPLICIT AND IMPLICIT AND TVD SCHEMES AND THEIR CONVERGENCE TO STEADY-STATE SOLUTIONS

P A Burton and P K Sweby

Numerical Analysis Report 5/95

DEPARTMENT OF MATHEMATICS

A DYNAMICAL APPROACH STUDY OF SOME EXPLICIT AND IMPLICIT TVD SCHEMES AND THEIR CONVERGENCE TO STEADY-STATE SOLUTIONS. [1]

P. A. Burton [2] & P. K. Sweby

Numerical Analysis Report 5/95

Department of Mathematics,
University of Reading,
P O Box 220,
Reading RG6 6AF.
U.K.

[1] Revised 12/95

[2] The first author wishes to acknowledge the financial support of the EPSRC. Award Ref. No. 94000952.

Abstract

A 1-D transonic flow model exhibiting multiple steady-states is used as a test problem to compare the results gained from explicit and implicit formulations of a high-resolution TVD scheme using a selection of flux limiters. It is shown how implicit schemes can converge to falsely stable steady solutions, i.e. stable solutions of the discretized equation which correspond to unstable solutions of the original ODE. It is also shown how the choice of flux limiter can affect convergence with certain limiters prone to suffer from residual plateauing whereby the residual error in the numerical solution decreases only so far before levelling off. A dynamics of discretization approach is used to study the effect the choice of limiter has on the dynamics of the scheme. It is shown how spurious asymptotic behaviour can be introduced which can cause fragmentation and shrinkage of the numerical basins of attraction. Finally, two methods for preventing residual plateauing are discussed, these are limiter-freezing and limiter-switching. A dynamical study puts the reliability of the limiter-freezing method into question.

1 Introduction

The need for accurate and efficient numerical schemes for the solution of systems of hyperbolic conservation laws, such as those arising in aerodynamics, has stimulated a great deal of research in recent years [15, 20]. One of the main stumbling blocks in the numerical solution of such problems is the inability of classical schemes to accurately reproduce features such as discontinuities, or shocks. Whereas first order schemes lead to the smearing out of such features, traditional second order schemes tend to suffer from overshoot and spurious oscillations in the vicinity of the shocks. This has lead to the development of high resolution Total Variation Diminishing (TVD) schemes, designed to produce oscillation free solutions whilst maintaining second order accuracy.

Although originally developed for time-dependent equations these schemes have found some success in application to steady-state problems. This often involves pseudo time-dependent techniques such as the method of lines, which uses spacial discretization to form a system of ODE equations in (artificial) time which are solved using either high order explicit schemes or (usually linearized) implicit schemes. It has been noted however that the devices used to achieve oscillation-free solutions, such as Flux Limiters [15], can sometimes serve to hinder, and even prevent, convergence to the steady-state. This leads to the phenomenon known as residual plateauing whereby the residual decreases only so far before levelling out [20, 21]. It is occasionally possible to remedy the effects of residual plateauing through the use of empirical techniques such as limiter freezing, whereby the value of the limiter function is fixed once plateauing occurs. Though sometimes adopted in practice this type of approach is at best a rather *ad hoc* solution and has yet to be put on any firm theoretical footing.

It has been widely shown [5, 9, 10, 17, 22, 23, 24, 25] that the dynamics of numerical discretizations can differ significantly from the dynamics of the original differential equations, the former possessing spurious asymptotic solutions, such as steady-states, periodic solutions and chaos, which are not admitted by latter. In addition, these spurious solutions, which can be either stable or unstable, can occur below as well as above the linear stability limit of the scheme. As described in [5, 17, 25] the basins of attraction of the spurious asymptotes, i.e. the domain of initial points whose solution curves all approach the same asymptotic state, can cause a dramatic distortion, shrinkage and segmentation of the basins of the true solution. The effect of this dependence on initial conditions is to allow the possibility of physically reasonable initial data leading, not only to divergent or non-convergent solutions, but also to plausible, yet spurious, steady-state solutions.

Yee & Sweby [25] demonstrated how the choice of implicit solver affected the dynamical behaviour of a selection of implicit schemes. It is the aim of this report to provide a similar analysis highlighting the effect the choice of flux limiter has on the dynamics of a TVD scheme applied to a simple one-dimensional scalar steady-state problem, in particular using a dynamical systems approach to investigate the barriers to convergence raised by certain limiters and a possible remedy.

The test problem, described in Section 2.1, arises from a paper by Embid, Goodman and Majda [4] on multiple steady-states for 1-D transonic flow problems. In order to provide a description of the problem and its solution, both

analytical and numerical, many of the results from the Embid paper are reproduced in Section 2. This includes highlighting phenomena such as convergence to falsely stable steady-state (whereby physically unstable solutions of the differential equation can be made stable by the numerical discretization) and also serves to describe the solutions obtained from a variety of classical first- and second-order schemes.

After a brief introduction to TVD schemes, Section 3 goes on to apply both explicit and implicit formulations to the scalar test problem, comparing results gained from a selection of typical flux limiter functions. It is shown how the choice of limiter can affect convergence, even to the point of preventing convergence altogether resulting in residual plateauing.

Section 4 provides a closer analysis of the differences in the behaviour of the various limiters. The test problem is reduced to a two-dimensional dynamical system allowing the schemes to be analysed in a dynamics of discretization context, using bifurcation and basins of attraction diagrams to describe the evolution of the solution for the two grid points lying either side of the shock.

Finally Section 5 describes two techniques, limiter freezing and limiter switching, used to combat the effects of residual plateauing. Results for the scalar test problem indicate significant improvements in the convergence of particular schemes using these techniques; a dynamics of discretization analysis, however, puts the effectiveness of the limiter freezing method into question.

2 Multiple Steady-states

The problem under consideration is the scalar equation

$$u_t + \left(\tfrac{1}{2}u^2\right)_x = g(x)u, \quad 0 \leq x \leq 1. \tag{2.1}$$

$$u(0,t) = u_0,\ u(1,t) = u_1.$$

It was put forward by Embid, Goodman and Majda [4] as a suitable 1-D test case for investigating multiple steady states for transonic flow calculations. After proving that multiple steady states exist for this problem, the paper went on to show how implicit numerical schemes, which are commonly used in steady-state applications because they allow large time-steps, can converge to physically unstable steady states.

Transonic flow problems are such that their solutions contain discontinuities (shocks) where the solution jumps from super- to sub-sonic flow (or vice versa). Any steady-state solution of equation (2.1), with boundary conditions of opposite sign, will therefore contain such a shock. The Rankine-Hugoniot jump condition for an admissible shock is given by

$$s = \frac{f(u^l) - f(u^r)}{u^l - u^r} = \frac{[f]}{[u]} \tag{2.2}$$

where s is the shock speed and u^l , u^r are the left and right branches of the solution either side of the shock. For equation (2.1) $f = \frac{1}{2}u^2$ and the jump condition reduces to

$$s = \frac{u^l + u^r}{2}.$$

For steady-state problems the shock is stationary, so the shock speed s=0. The solution will therefore contain a shock at points where

$$p(x) = \tfrac{1}{2}(u^l(x) + u^r(x)) = 0. \tag{2.3}$$

It is possible to construct the left and right branches of the solution of equation (2.1) by noting that for a steady-state solution $u_t = 0$. Rewriting $\left(\frac{1}{2}u^2\right)_x$ as uu_x it can be observed that u^l and u^r must satisfy the ODE

$$u_x = g(x),$$

giving

$$\begin{aligned} u^l(x) &= u_0 + G(x) \\ u^r(x) &= u_1 + G(x) - G_1 \end{aligned}$$

where

$$G(x) = \int_0^x g(s)ds, \quad G_1 = \int_0^1 g(s)ds.$$

Putting these expressions for u^l and u^r into equation (2.3) it can be seen that shocks will occur at points $x = x_j$, where the x_j are roots of

$$p(x) = \tfrac{1}{2}(u_0 + u_1 - G_1) + G(x) = 0.$$

The steady solution of equation (2.1) is therefore

$$u(x) = \begin{cases} u^l(x) & \text{when } x < x_j, \\ u^r(x) & \text{when } x > x_j, \end{cases} \tag{2.4}$$

which can be shown to satisfy the entropy condition, $u^l(x) > u^r(x)$, for all x provided u_0, u_1 and G_1 satisfy the condition

$$u_0 > u_1 - G_1.$$

This implies that if $p(x)$ has multiple distinct roots then there will be multiple entropy-satisfying steady-state solutions. Furthermore, for a problem with fixed boundary conditions, it is possible to choose the source term, $g(x)$, to give an arbitrarily large number of entropy satisfying steady solutions.

Both stable and (physically) unstable steady-state solutions can occur which can lead to problems when the equation is solved numerically. It has been noted for a variety of schemes and problems [5, 10, 17, 22, 23, 24, 25] that the stability of the solutions gained from discretized equations can differ from those of the original DE, causing possible convergence to unstable solutions of the underlying differential equation. Such solutions are called 'falsely stable solutions' of the discretized equations, or 'physically unstable solutions' of the DE.

In the next section this effect is investigated, following the work of Embid *et al* [4], using a particular test problem and a variety of schemes.

2.1 The Scalar Test Problem

The test problem presented in [4] for the study of the behaviour of numerical schemes in multiple steady-state applications was

$$u_t + \left(\tfrac{1}{2}u^2\right)_x = (6x - 3)u, \quad (0 < x < 1), \tag{2.5}$$

$$u_0 = 1, \quad u_1 = -0.1.$$

Here $p(x)$ has two distinct roots, $x_1 = 0.18$ and $x_2 = 0.82$, so there are two entropy-satisfying steady solutions. One has a standing shock at $x = x_1$ and can be shown to be stable, the other has a standing shock at $x = x_2$ which can be shown to be unstable (see [4] for details). On either side of the shock the solution follows the solution curves

$$\begin{array}{rcll} u^l(x) & = & 3x(x-1)+1 & x < x_j, \\ u^r(x) & = & 3x(x-1)-0.1 & x > x_j, \end{array} \tag{2.6}$$

for $j = 1, 2$.

Equation (2.5) was solved numerically using three methods, the first order implicit upwind scheme of Engquist & Osher, its second order counterpart, and the second order explicit MacCormack scheme. All three schemes use time stepping as a relaxation method for solving the steady-state equation.

a) **The First Order Implicit E-O Upwind Scheme**

The upwind differencing of Engquist & Osher [2, 3] is combined with backwards implicit Euler time differencing to give

$$u_k{}^{n+1} = -\lambda D^u f(u_k^{n+1}) + \Delta t g(x) u_k^{n+1}, \tag{2.7}$$

where,

$$D^u f(u_k) = f_{k+1}^- + f_k^+ - f_k^- - f_{k-1}^+, \tag{2.8}$$

and λ is the mesh ratio $\frac{\Delta t}{\Delta x}$.

For convex f, as in the test problem (2.5),

$$f_k^+ = f(\max(u_k, \bar{u})), \tag{2.9}$$
$$f_k^- = f(\min(u_k, \bar{u})), \tag{2.10}$$

where $\bar{u}$ is the sonic value satisfying $f'(\bar{u}) = 0$.

The implicit equations are solved using linearization, whereby

$$S_k^{n+1} = -\lambda D^u f(u_k^{n+1}) + \Delta t g(x) u_k^{n+1}$$

is expanded as

$$S_k^{n+1} = S_k^n + J(u_k^n)\left[u_k^{n+1} - u_k^n\right],$$

and where $J(u_k^n)$ is the Jacobian $\frac{\partial S_k^n}{\partial u^n}$.

Hence the linearized implicit scheme takes the form

$$(I - J(u_k^n)) \cdot \left[u_k^{n+1} - u_k^n\right] = -\lambda D^u f(u_k^n) + \Delta t g(x) u_k^n. \tag{2.11}$$

This gives a three point scheme which can be used at all interior grid points, with points on the boundary being specified by the boundary conditions.

b) **The Second Order Upwind Scheme**

Second order upwind differencing is combined with backward implicit Euler time differencing to give

$$u_k^{n+1} = u_k^n - \lambda D^{uu} f(u_k^{n+1}) + \Delta t g(x) u_k^{n+1}, \tag{2.12}$$

where

$$D^{uu} f(u_k^n) = D^{++} f_k^- + D^{--} f_k^+, \tag{2.13}$$

$$D^{++} f_k^- = -\tfrac{1}{2} f_{k+2}^- + 2 f_{k+1}^- - \frac{3}{2} f_k^-, \tag{2.14}$$
$$D^{--} f_k^+ = \tfrac{1}{2} f_{k-2}^+ - 2 f_{k-1}^+ + \frac{3}{2} f_k^+, \tag{2.15}$$

and where f_k^+ and f_k^- are as defined in (2.9) and (2.10) for the first order scheme.

As with the first order scheme linearization is used to solve the implicit equations. In order to avoid inverting the pentadiagonal Jacobian, J', resulting from the 5-point scheme (2.12), Embid *et al* recommend using a tridiagonal Jacobian, M, which is a linear combination of the first order Jacobian J, from (2.11), and the tridiagonal restriction of J', denoted J'' (obtained by setting the outer diagonal elements of J' to zero). That is

$$M(\omega) = \omega J'' + (1-\omega)J, \tag{2.16}$$

where ω is a parameter chosen to maximise the bound on λ . Embid *et al* report that this choice of Jacobian gives a much larger stability bound on λ than simply using the first order Jacobian J (equivalent to setting $\omega = 0$). Since this is a 5-point scheme it cannot be used at grid points adjacent to the boundaries, at these points first order upwind differencing is used.

c) **The Second Order Explicit MacCormack Scheme**

The second order MacCormack scheme, adapted to include the source term in equation (2.1), is given by

$$\begin{aligned} v_k^{n+1} &= u_k^n - \lambda D^+ f(u_k^n) + \Delta t g(x) u_k^n, \\ u_k^{n+1} &= u_k^n - \tfrac{1}{2}\lambda \left[D^- f(v_k^{n+1}) + D^+ f(u_k^n) \right] \\ &\quad + \tfrac{1}{2}\Delta t g(x) \left[u_k^n + v_k^{n+1} \right], \end{aligned} \tag{2.17}$$

where $D^+ f_k = f_{k+1} - f_k$ and $D^- f_k = f_k - f_{k-1}$.

This is a 2-step predictor-corrector method with forward differencing in the predictor and backward differencing in the corrector. In order to preserve accuracy at the right boundary the value v^{n+1} is used instead of the boundary condition $u(1,t) = u_1$.

2.2 Computation and Results

The three schemes listed above were used to solve equation (2.5) which has two entropy satisfying steady solutions, one with a stable standing shock at $x_1 = 0.18$ and one with an unstable standing shock at $x_2 = 0.82$.

In all the results that follow the region $0 \leq x \leq 1$ was discretised using 40 grid points, so that $\Delta x = 0.025$. Where appropriate each scheme was run using a high Courant number, $c = a_{max}\lambda$, whilst still maintaining stability. For this problem the fastest wave speed, a_{max}, occurs at the left boundary where $a = \frac{1}{2}$.

Initial conditions were chosen to follow the solution branches

$$u(x) = \begin{cases} u^l(x) & x < x_0, \\ u^r(x) & x > x_0, \end{cases}$$

for some choice of initial jump position x_0. The steady solutions were then calculated by marching in time until the convergence criterion

$$\sum_k \left| u_k^{n+1} - u_k^n \right| \leq 10^{-15}$$

was satisfied.

Accuracy of the numerical approximations. Figures 2.1, 2.2 and 2.3 show the results of taking initial conditions with a jump at $x_0 = x_1$ for the first order, second order and MacCormack schemes respectively. The solid lines represent the solution branches $u^l(x)$ and $u^r(x)$, and the dots represent the computed solution. The mark on the x-axis indicates the value of x_0 chosen for the initial jump location.

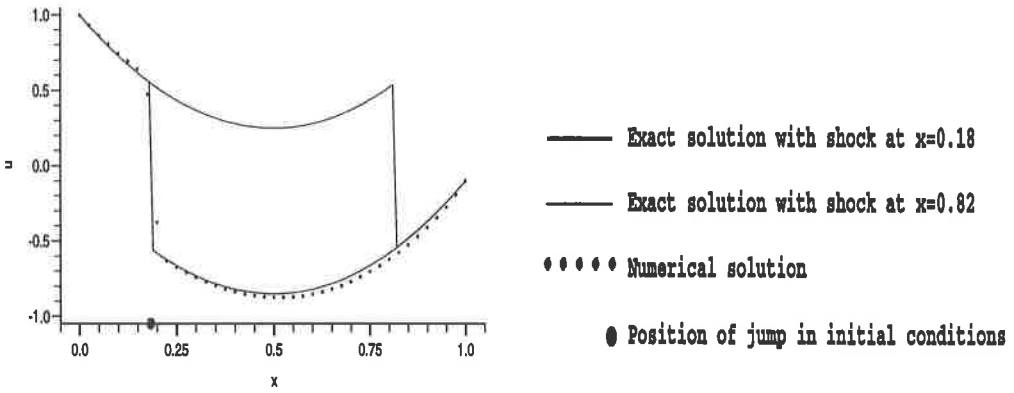

Figure 2.1: E-O upwind scheme, c=300

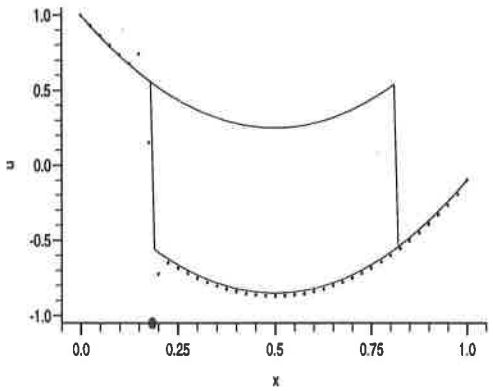

Figure 2.2: 2nd order upwind scheme, c=300

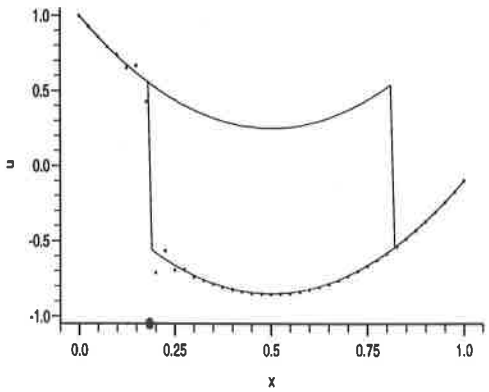

Figure 2.3: Explicit MacCormack scheme, c=0.25

All three schemes converge to the stable shock solution at x_1. The first order scheme, calculated with Courant number $c = 300$, displays low accuracy but, being monotone, does not produce numerical oscillations around the shock. The second order scheme, calculated using $c = 300$ and $\omega = 0.045$, demonstrates a higher degree of accuracy over the majority of the region, but produces a single point of overshoot either side of the shock. This behaviour is characteristic of the scheme. The explicit MacCormack scheme, with $c = \frac{1}{4}$, displays much greater accuracy compared with the implicit schemes but suffers from severe oscillations around the shock. Embid *et al* report that this is a particularly severe test of the scheme since no artificial damping was used.

The relatively low accuracy of both implicit upwind schemes is due in part to

the proximity of the right boundary value, $u = -0.1$, to the sonic point, $u = 0$. If the solution is calculated numerically for $0 \leq x \leq 0.9$ the influence of the sonic point is removed and the two schemes display much more accurate results (see Figures 2.4 and 2.5).

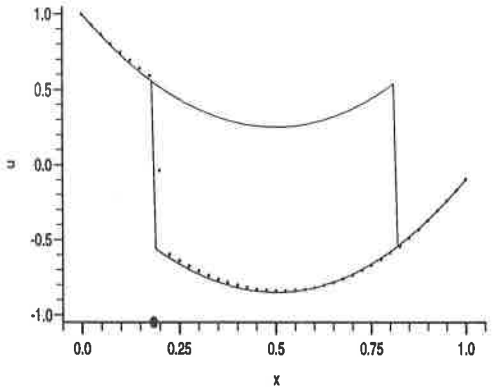

Figure 2.4: E-O upwind scheme, c=300, $0 < x < 0.9$

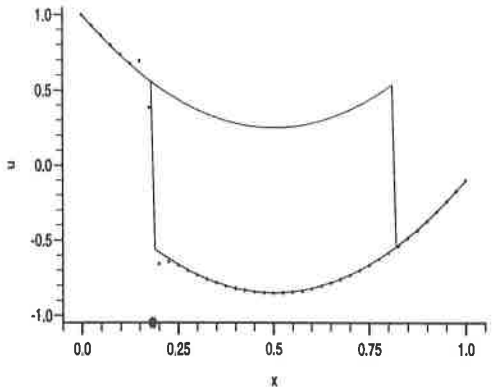

Figure 2.5: 2nd order upwind scheme, c=300, $0 < x < 0.9$

Convergence to falsely stable steady solutions. If initial data is chosen with a jump at or near the unstable shock at $x_2 = 0.82$, the implicit schemes can be shown to converge to the physically unstable steady state. Figure 2.6 shows the result of using the first order scheme with $c = 24$ and with an initial jump at $x_0 = 0.82$. Although the accuracy is very low the scheme has converged to the physically unstable solution.

Systematic numerical experiments were performed by taking initial data with a jump at

$$x_0 = dx_1 + (1 - d)x_2, \tag{2.18}$$

for some parameter, d.

The results indicated three ranges of Courant number. For $c < c_i$ the numerical solution converged to the physically stable steady solution, leading to non-convergence. For values of c in the range $c_i < c < c_j$ the time integration became unstable. Finally, for $c > c_j$ the numerical solution converged to the physically unstable steady solution. Table 2.1 gives experimental values of c_i and c_j using the first order scheme with a range of d values.

d	0.0	0.1	0.2	0.3	0.4
c_i	10.5	12.5	18.0	25.0	59.5
c_j	21.0	23.5	30.5	38.0	60.0

Table 2.1: Courant ranges for the convergence of the 1st order E-O scheme

The second order scheme displays similar behaviour. Figure 2.7 shows the result of taking $c = 300$, $\omega = 0.045$ and initial jump $x_0 = 0.82$. These falsely stable solutions are approximations to exact entropy satisfying but physically unstable solutions of equation (2.5).

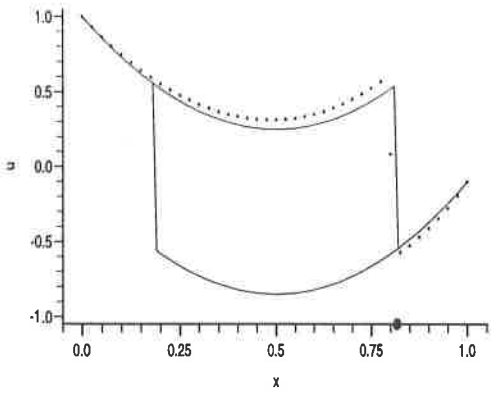

Figure 2.6: E-O upwind scheme, c=24

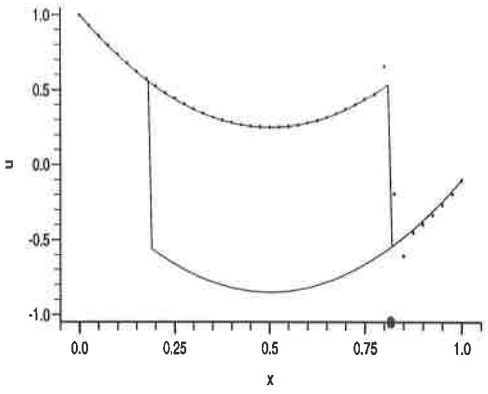

Figure 2.7: 2nd order upwind scheme, c=300

The results in this section illustrated how three standard schemes perform for a simple 1-D transonic flow test problem possessing multiple steady-states. It was shown how implicit schemes, although advantageous in steady-state applications because they allow large time-steps to be taken, can converge to physically unstable steady solutions of the differential equation for certain values of Courant number and initial conditions. In addition it was illustrated how conventional higher order schemes produce solutions with spurious oscillations in the neighbourhood of shocks.

In the following section a particular class of schemes will be considered which give second order accurate solutions but without producing spurious oscillations. These are Total Variation Diminishing, or TVD, schemes. These schemes will be applied to the test problem (2.5) and their bevaviour analysed as they approach steady-state.

3 TVD Schemes

Total Variation Diminishing (TVD) schemes are designed to maintain high resolution solutions whilst avoiding the spurious oscillations produced by more conventional high order schemes. They are based on an important property of scalar conservation laws, that the total variation of any solution

$$TV = \int |u_x|\, dx$$

does not increase in time (Lax, 1973).

The total variation (TV) of a numerical solution of a scalar conservation law is given by

$$TV(u) = \sum_k |u_{k+1} - u_k| \,. \tag{3.1}$$

If the total variation is such that it satisfies the relation

$$TV(u^{n+1}) \leq TV(u^n) \tag{3.2}$$

then the scheme is said to be total variation diminishing [6, 7]. This property ensures that no new local maxima and minima are produced (which would increase the total variation) and hence that no spurious oscillations can occur.

An important class of TVD schemes are E-schemes [13, 18] which can be shown to be entropy satisfying and at most first order accurate. In fact no second or higher order accurate constant coefficient scheme can be TVD. In order to acheive second order accuracy whilst maintaining TVD it is therefore necessary to use schemes which depend on the solution at each time-step, i.e. schemes with nonlinear coefficients. One method of acheiving this is to take a first order E-scheme and make it second order accurate by adding an anti-diffusive flux term, which is constrained in some nonlinear way, in order to maintain TVD. This approach, called the Flux Limiter method [14, 15], gives the TVD scheme the following form:

$$\begin{aligned} u_k^{n+1} \;=\; u_k^n \;&-\; \lambda\Delta_- h^E_{k+\frac{1}{2}} \qquad\qquad (\ 1^{st}\text{order E-scheme}\ ) \\ &-\; \underbrace{\lambda\Delta_- \left\{ \phi(r_k^+)\alpha^+_{k+\frac{1}{2}}(\Delta f_{k+\frac{1}{2}})^+ - \phi(r^-_{k+1})\alpha^-_{k+\frac{1}{2}}(\Delta f_{k+\frac{1}{2}})^- \right\}}_{\text{limited anti-diffusive flux term}} \end{aligned} \tag{3.3}$$

where, for time accurate problems,

$$\alpha^\pm_{k+\frac{1}{2}} = \tfrac{1}{2}(1 \mp |v^\pm_{k+\frac{1}{2}}|),$$

$$v^\pm_{k+\frac{1}{2}} = \frac{\lambda(\Delta f_{k+\frac{1}{2}})^\pm}{\Delta u_{k+\frac{1}{2}}},$$

$$(\Delta f_{k+\frac{1}{2}})^+ = -\left(h^E_{k+\frac{1}{2}} - f(u_{k+1})\right), \quad (\Delta f_{k+\frac{1}{2}})^- = \left(h^E_{k+\frac{1}{2}} - f(u_k)\right),$$

$$r_k^\pm = \left[\frac{\alpha^\pm_{k-\frac{1}{2}}(\Delta f_{k-\frac{1}{2}})^\pm}{\alpha^\pm_{k+\frac{1}{2}}(\Delta f_{k+\frac{1}{2}})^\pm}\right]^{\pm 1} \quad \text{is a solution monitor, and}$$

$\phi(r)$ is the flux limiter designed to maintain TVD.

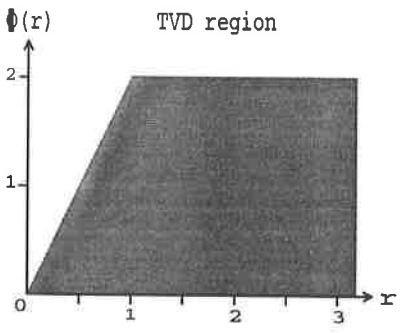

Figure 3.1

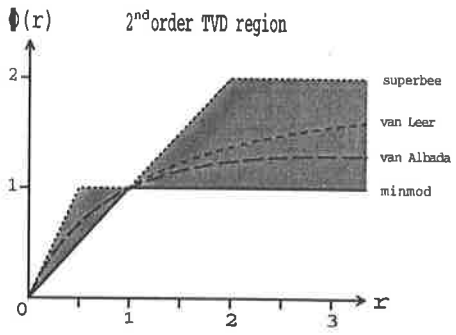

Figure 3.2

The limiter $\phi(r)$ can be chosen in many ways, but must lie within a specified region in order to preserve the TVD property (Figure 3.1). As a further constraint the shaded area in Figure 3.2 describes the region within which $\phi(r)$ must lie to ensure second order accuracy [15].

Some examples of flux limiters are

$$\phi_1(r) = \max(0, \min(r, 1)) \text{ — Roe's } \textbf{minmod} \text{ limiter,} \tag{3.4}$$

$$\phi_2(r) = \max(0, \min(2r, 1), \min(r, 2)) \text{ — Roe's } \textbf{superbee} \text{ limiter,} \tag{3.5}$$

$$\phi_{VL}(r) = \frac{r + |r|}{1 + |r|} \text{ — } \textbf{van Leer}\text{'s limiter,} \tag{3.6}$$

$$\phi_{VA}(r) = \frac{r + r^2}{1 + r^2} \text{ — } \textbf{van Albada}\text{'s limiter,} \tag{3.7}$$

all of which lie within the second order TVD region (Figure 3.2).

It is important to note that the TVD property only holds for homogeneous hyperbolic scalar conservation laws and will not ensure non-oscillatory solutions for problems involving source terms, such as the test problem (2.5). The use of the TVD formulation for non-homogeneous problems however remains a sound criterion on which to base a scheme and can still be used, provided the source term is properly treated, to produce oscillation free solutions for certain special cases (see Sweby [16] and Yee & LeVeque [12]).

3.1 Computation and Results

Both explicit and implicit formulations of the TVD scheme (3.3) were used to solve the test problem (2.5). The E-scheme used in the calculations used the first order Engquist-Osher differencing given in Section 2.1a, so that $h^E_{k+\frac{1}{2}} = f^-_{k+1} + f^+_k$. It should be noted that for steady-state problems $\alpha^\pm$ should be replaced by $a = \frac{1}{2}$, giving a method of lines formulation and thus avoiding dependence of the steady solution on the time step Δt. Although the scheme loses some time accuracy it maintains spacial accuracy. The schemes therefore become

(a) **Explicit Scheme**

$$\begin{aligned} u_k^{n+1} &= u_k^n - \lambda\Delta_- \left(f^-_{k+1} + f^+_k\right) + \Delta t g(x) u_k^n \\ &\quad -\tfrac{1}{2}\lambda\Delta_- \left[\phi(r^+_k)(\Delta f_{k+\frac{1}{2}})^+ - \phi(r^-_{k+1})(\Delta f_{k+\frac{1}{2}})^-\right]. \end{aligned} \tag{3.8}$$

(b) **Linearized Implicit Scheme**

$$\begin{aligned} J(u_k^n)[u_k^{n+1} - u_k^n] &= -\lambda\Delta_-(f_{k+1}^- + f_k^+) + \Delta t g(x) u_k^n \\ &\quad -\tfrac{1}{2}\lambda\Delta_- \left[\phi(r_k^+)(\Delta f_{k+\frac{1}{2}})^+ - \phi(r_{k+1}^-)(\Delta f_{k+\frac{1}{2}})^-\right]. \end{aligned} \tag{3.9}$$

Rather than attempting to calculate the Jacobian of the 5-point limited flux terms for the linearized implicit scheme, the first order tridiagonal Jacobian from equation (2.11) has been used at all internal grid points.

Experiments have been carried out for both schemes using each of the flux limiters (3.4)–(3.7), and also for first order explicit and implicit E-O schemes (equivalent to setting $\phi = 0$ in equations (3.8) and (3.9) above). Throughout this section convergence was determined using the same criterion as in section (2.2), namely that the numerical solution satisfies the following bound on the residual

$$\sum_k \left|u_k^{n+1} - u_k^n\right| \leq 10^{-15}.$$

Initial conditions were taken with jumps at either $x_0 = x_1 = 0.18$, or $x_0 = x_2 = 0.82$, marching in time until the convergence criterion was satisfied or the number of iterations, n, exceeded $n = 2000$.

3.1.1 Explicit Schemes

Table 3.1 illustrates how the convergence behaviour of the five explicit TVD schemes is dependent upon the Courant number $c = a\lambda$. For Courant number $c \leq c_i$ the numerical solution converges to the stable steady shock at $x = x_1$, with the number of iterations required for convergence decreasing as $c \to c_i$. For $c_i < c < c_j$ the schemes do not converge within the specified iteration limit $n = 2000$. For $c \geq c_j$ the schemes are unstable. As would be expected the limited schemes have a smaller stability range than the first order scheme on which they are based.

scheme	c_i	c_j
E-O	0.65	0.9
minmod	0.5	0.75
superbee	—	0.7
van Leer	0.6	0.7
van Albada	0.6	0.7

Table 3.1: Convergence regions for the explicit TVD schemes.

The results gained from the explicit schemes by taking $c = 0.4$ and initial jumps at $x_0 = 0.18$ are shown in Figures 3.3–3.7. Although the TVD schemes do not exhibit the same accuracy as the second order upwind scheme, Figure 2.2, or the second order explicit MacCormack scheme, Figure 2.3, nor do they suffer from the spurious oscillations inherent in the second order schemes of Section 2.1.

It was found that the choice of initial conditions did not affect the final solutions or the values of c_i and c_j given in the table.

The most striking feature of the table is that the explicit superbee scheme does not converge for any value of c. Some insight into the cause for this can be gained by considering the behaviour of the residual $r^n = |u^{n+1} - u^n|$ as a function of the iteration number n, as illustrated in Figures 3.3–3.7. In the case of the superbee limited scheme, Figure 3.4, the residual drops initially but then levels off, oscillating around $r = 1 \times 10^{-3}$. This effect, often refered to as residual plateauing, is the cause of the non-convergence of the schemes for $c_i < c < c_j$. In some cases the residual does not level off completely, but decreases at a very gradual rate, resulting in very slow convergence. It is believed that this behaviour can be aggravated by the use of the nonlinear limiter functions used in the schemes.

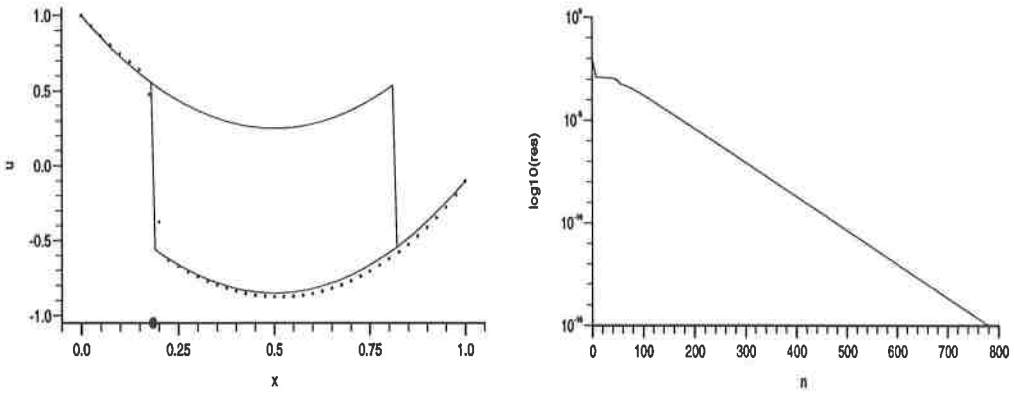

Figure 3.3: 1st order explicit E-O scheme, c=0.4

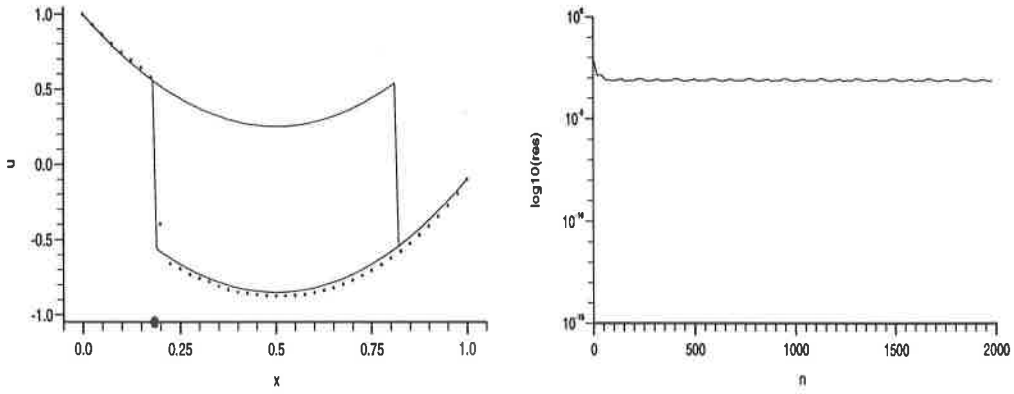

Figure 3.4: Explicit TVD superbee scheme, c=0.4

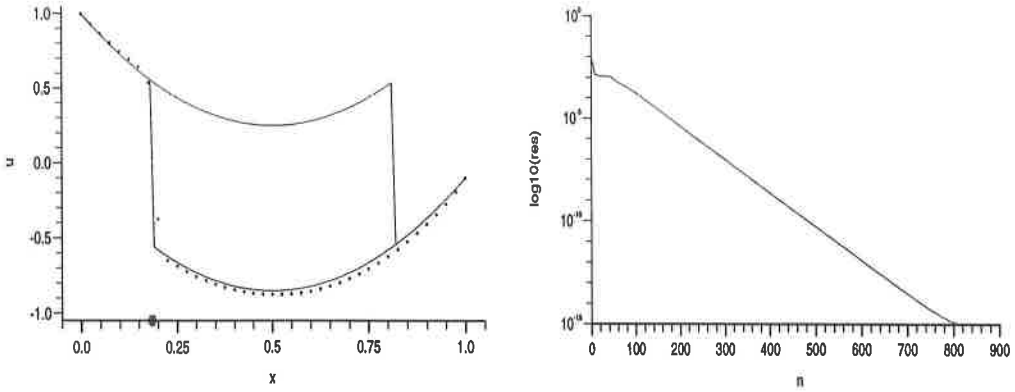

Figure 3.5: Explicit TVD minmod scheme, c=0.4

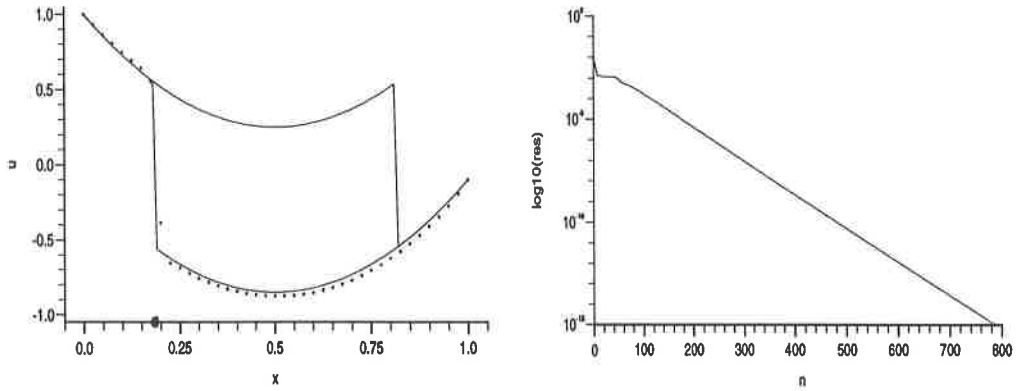

Figure 3.6: Explicit TVD van Leer scheme, c=0.4

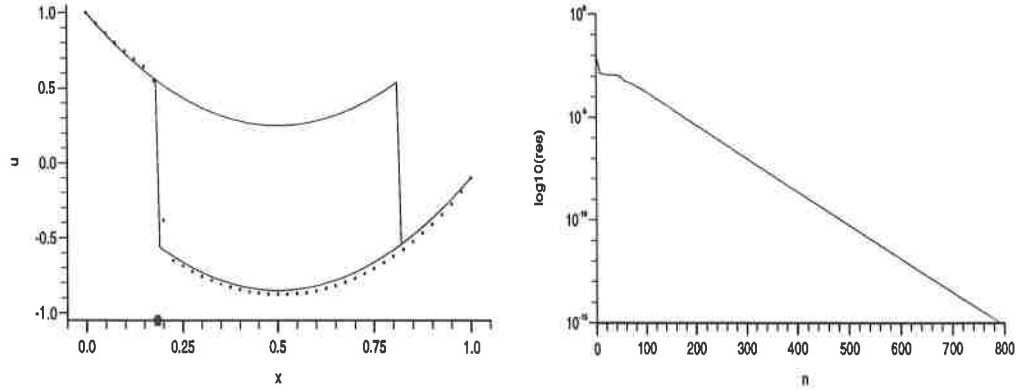

Figure 3.7: Explicit TVD van Albada scheme, c=0.4

3.1.2 Implicit Schemes

Unlike the explicit schemes, the choice of initial jump position x_0 can affect the numerical solution of the implicit schemes for certain values of c, causing convergence to falsely stable steady-states. Full experimental analysis of the

effect on convergence of different initial jump positions, like that described in Table 2.1, was not performed. However tests were made with two initial jump positions, $x_0 = x_1$ and $x_0 = x_2$. Results for these two cases are described below. Experiments were performed with Courant numbers in the range $\frac{1}{2} \leq c \leq 300$.

a) $x_0 = x_1$. Figures 3.8–3.12 illustrate the accuracy of the limited TVD schemes for $c = 300$ with initial jump position $x_0 = 0.18$, together with graphs of the residual, $r(n) = |u^{n+1} - u^n|$. The first order E-O sceme and the second order minmod and van Albada schemes all converged within the specified number of iterations, with the second order TVD schemes displaying the greater accuracy.

The superbee and van Leer schemes however have not converged for $c = 300$, as can be seen by the plateauing of the residuals in Figures 3.9 and 3.11. Experiments have shown that the superbee limited scheme gives fastest convergence when $c = 5$, with the number of iterations slowly increasing as c increases until $n > 2000$ when $c = 300$. The behaviour of the van Leer scheme is more abrupt, with the scheme going from fastest convergence for $c = 5.5$, to non-convergence for $c = 6$. It is worth noting that these two schemes do eventually recover, but only for very large values of c.

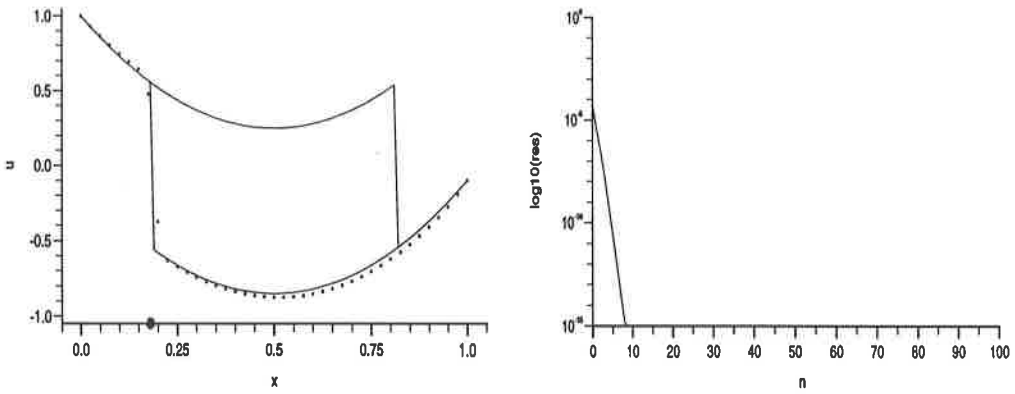

Figure 3.8: 1st order implicit E-O scheme, c=300

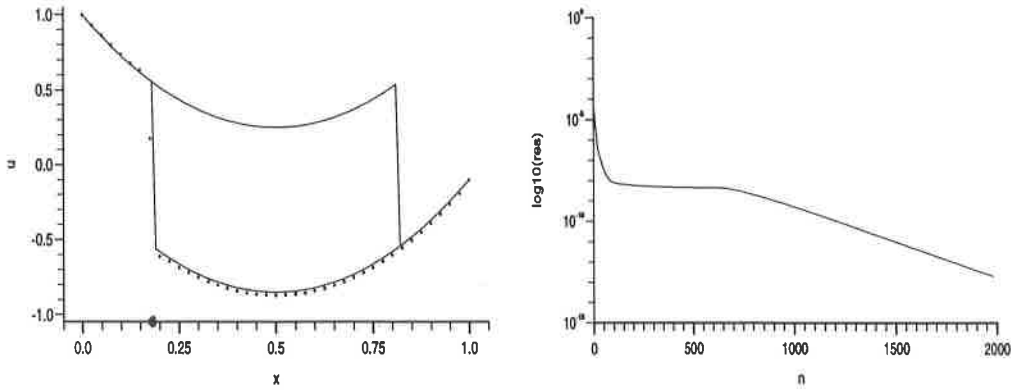

Figure 3.9: Implicit TVD superbee scheme, c=300

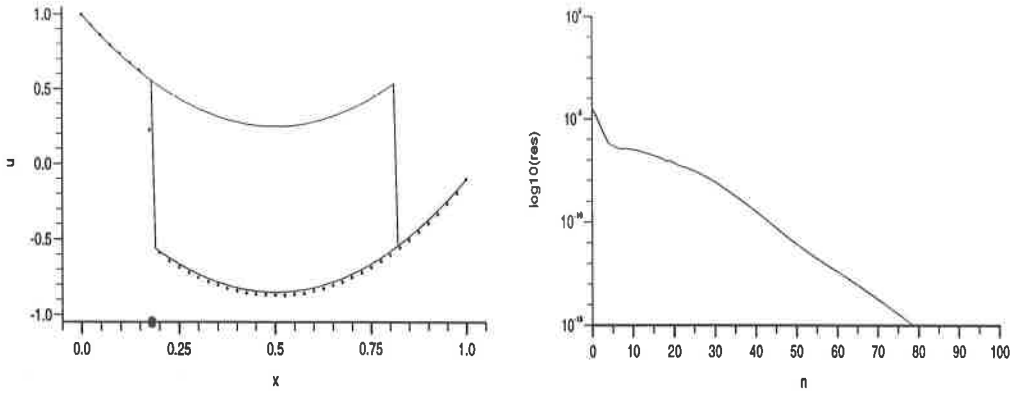

Figure 3.10: Implicit TVD minmod scheme, c=300

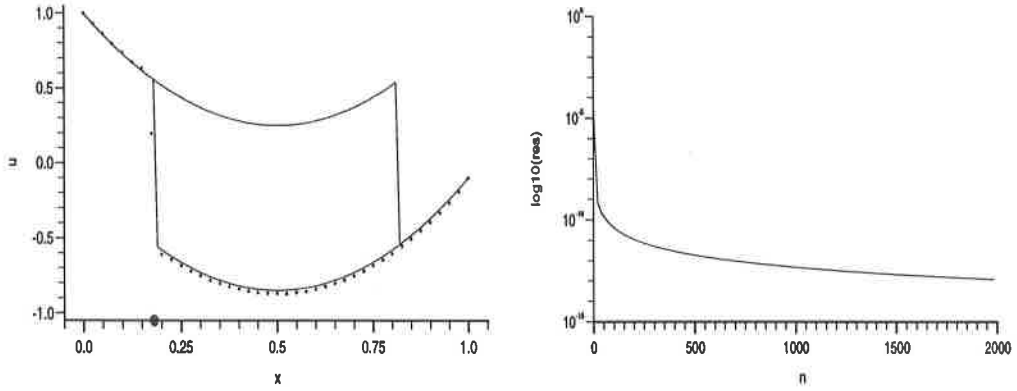

Figure 3.11: Implicit TVD van Leer scheme, c=300

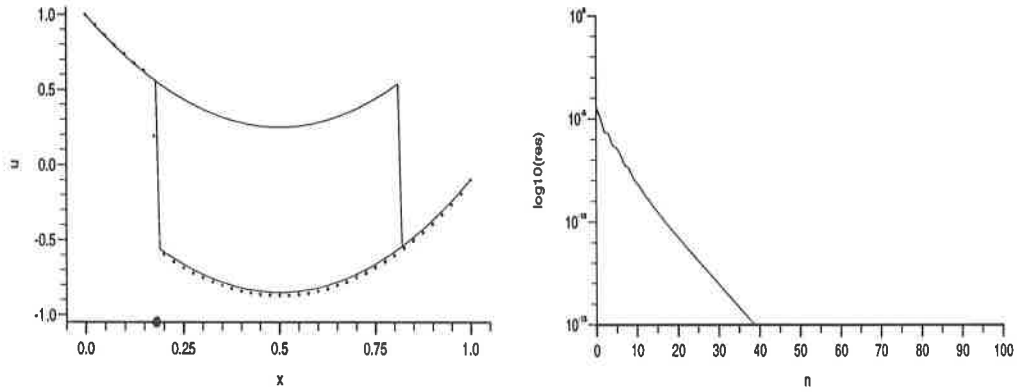

Figure 3.12: Implicit TVD van Albada scheme, c=300

b) $x_0 = x_2$. With an initial jump located at or near the unstable shock at $x_2 = 0.82$ the implicit schemes demonstrate similar behaviour to that of the implicit schemes in Section 2, i.e. for certain values of Courant number the schemes converge to the falsely stable steady solution.

In Section 2 it was noted that for $c < 11$ the first order E-O scheme converges to the physically stable solution which has a shock at $x = x_1$ (Figure 2.1). For $11 \leq c \leq 22.5$ the time integration became unstable, causing non-convergence. For $c > 22.5$ the E-O scheme converges to the falsely stable solution with a shock at x_2 (Figure 2.6). Since all of the flux limiter scheme being discussed are based

on the first order E-O scheme they all exhibit similar instabilities, i.e. the solution blows up for c in the range $11 \leq c \leq 21$.

For $c < 11$ all the schemes approach the stable steady solution, and for $c > 21$ they all approach the unstable steady solution. Table 3.2 gives the values of c for which each of the schemes converge to x_1 and x_2, the stable and falsely stable solutions respectively.

scheme	converges to x_1	converges to x_2
E-O	$c < 11$	$c \geq 22.5$
minmod	$c < 11$	$c \geq 21.5$
superbee	$c < 11$	—
van Leer	—	—
van Albada	$c < 11$	$c \geq 22.5$

Table 3.2: convergence regions for the implicit TVD schemes.

Figures 3.13–3.22 show solutions with residual graphs at $c = 10$ and $c = 300$ for the minmod, superbee, van Leer and van Albada limited schemes respectively. As with the explicit scheme the implicit superbee scheme suffers from residual plateauing, in this case for $c > 21$ when it is approaching the falsely stable steady solution (Figure 3.19). In addition, the van Leer scheme suffers from residual plateauing for all values of c (within the range $c \leq 300$), Figures 3.16 and 3.21. The minmod and van Albada schemes appear not to suffer from this problem.

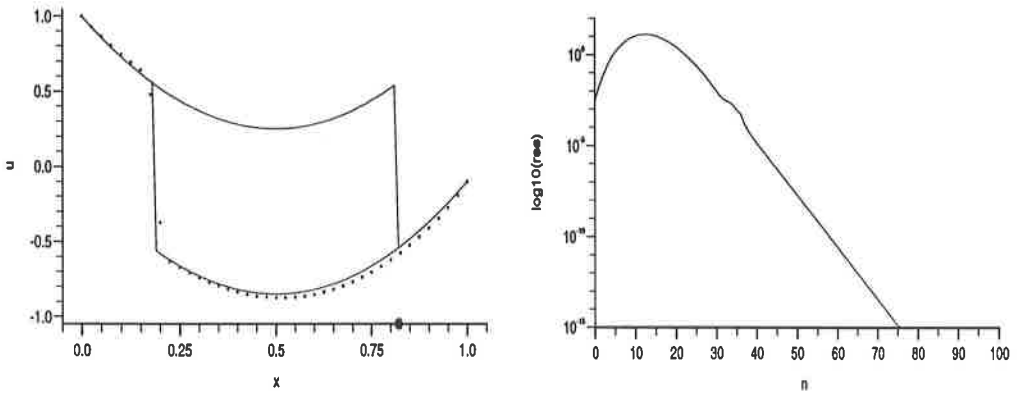

Figure 3.13: 1st order implicit E-O scheme, c=10

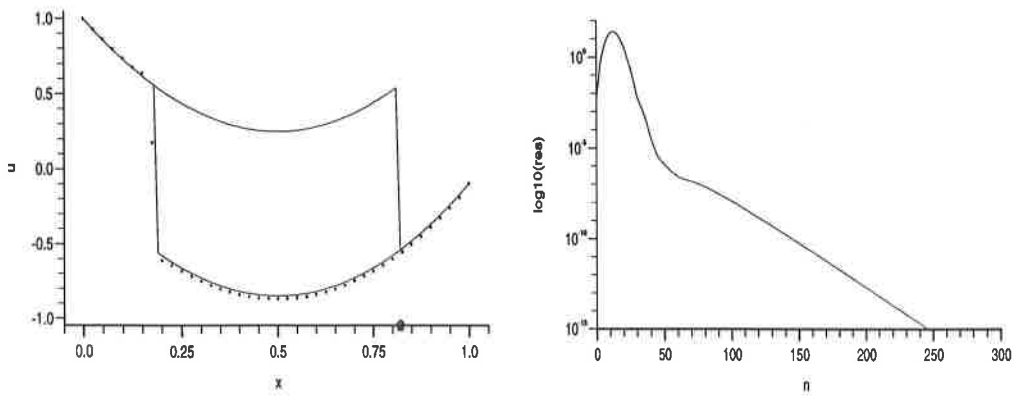

Figure 3.14: Implicit TVD superbee scheme, c=10

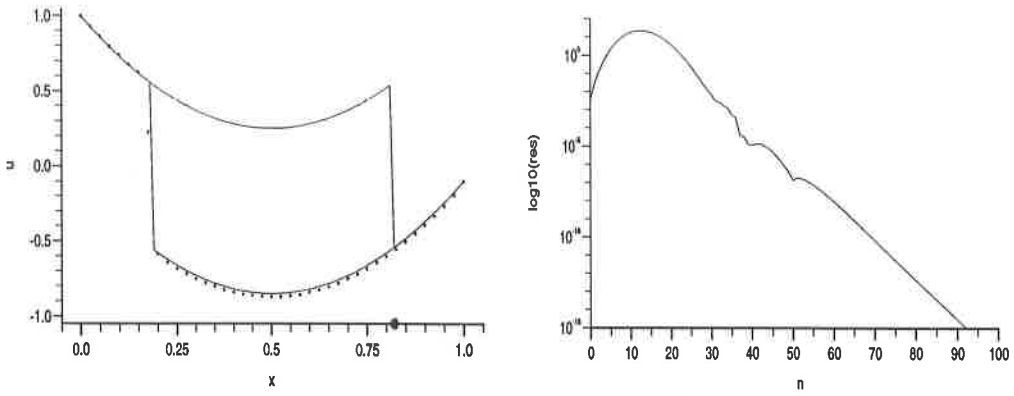

Figure 3.15: Implicit TVD minmod scheme, c=10

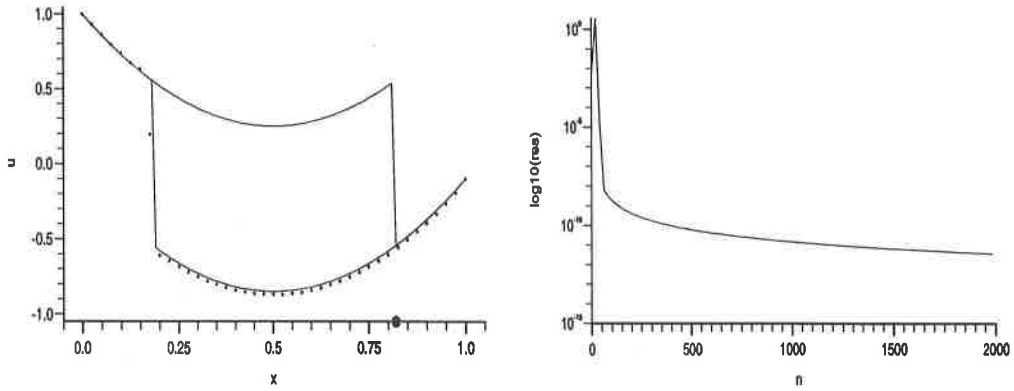

Figure 3.16: Implicit TVD van Leer scheme, c=10

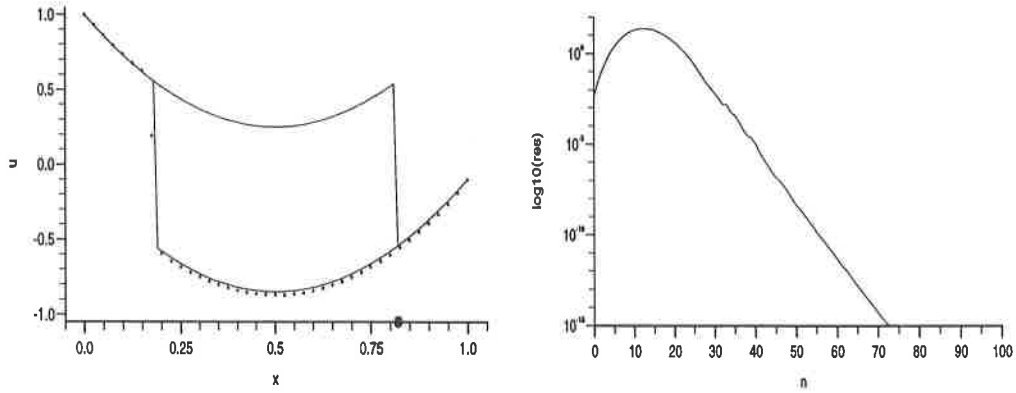

Figure 3.17: Implicit TVD van Albada scheme, c=10

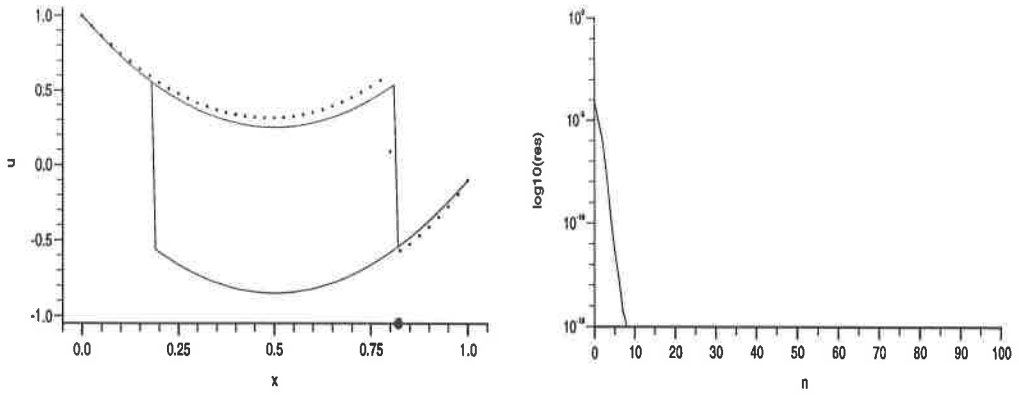

Figure 3.18: 1st order implicit E-O scheme, c=300

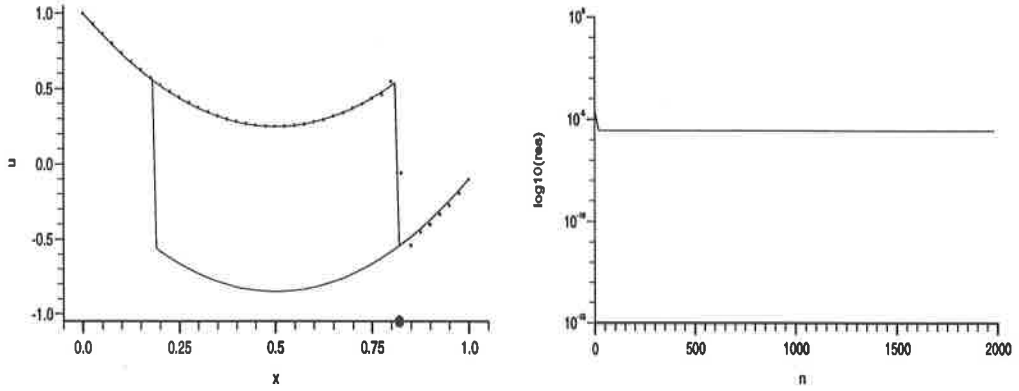

Figure 3.19: Implicit TVD superbee scheme, c=300

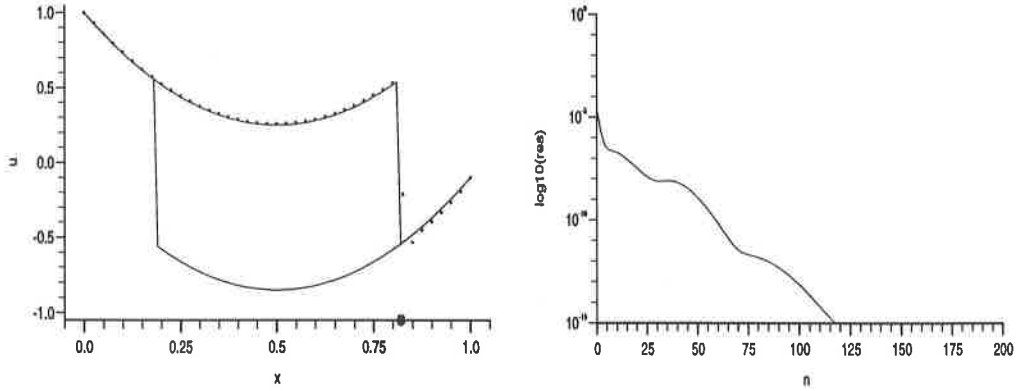

Figure 3.20: Implicit TVD minmod scheme, c=300

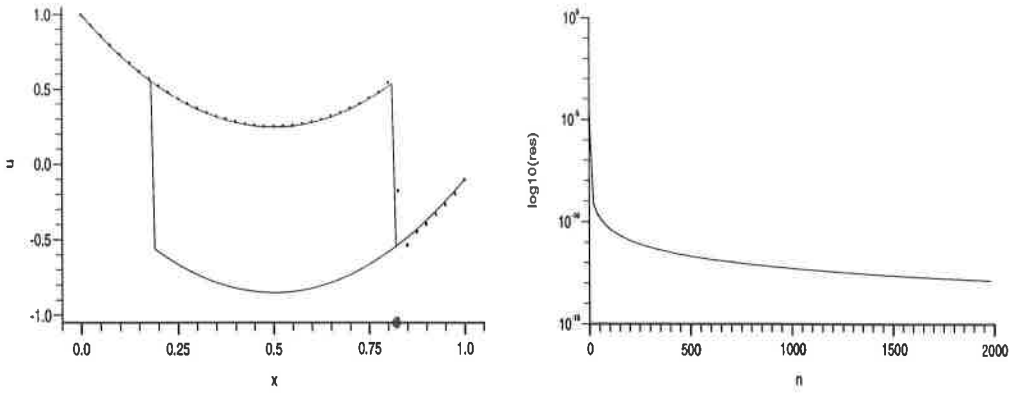

Figure 3.21: Implicit TVD van Leer scheme, c=300

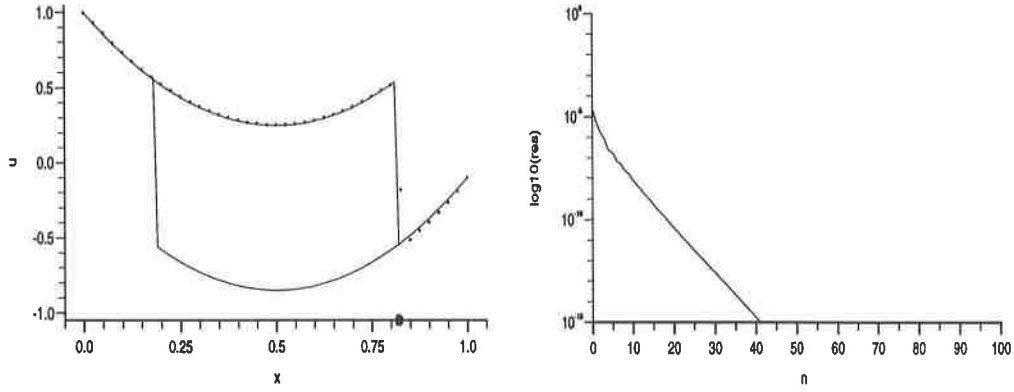

Figure 3.22: Implicit TVD van Albada scheme, c=300

The phenomenon of residual plateauing is believed to be linked to the stability of the limiter functions used in the TVD schemes [20, 21]. The superbee and van Leer limiters both lie towards the top of the TVD region (Figure 3.2), leading to larger contributions from the second order terms in the scheme. This makes the scheme more compressive, giving higher resolution at the shocks than if the less compressive minmod and van Albada limiters were used, both of which lie toward the bottom of the TVD region. However, the added influence of the second order terms also makes the scheme more unstable which, for inhomogeneous problems such as equation 2.5, can cause oscillations in the solution and can lead to residual plateauing.

In the following section a dynamics of discretization approach is applied to give a more detailed description of the influence the limiter functions have on the solution of the steady-state problem.

4 Dynamics of Discretization

The basic idea of this approach is to treat the numerical scheme as a discrete dynamical system. The behaviour of a particular quantity is monitored as a parameter, usually dependant on the time-step, is varied. The behaviour of the system can be represented graphically in the form of bifurcation diagrams, which describe the evolution of fixed points of the system, and basins of attraction, the sets of initial conditions which converge to the same asymptotic state.

This technique is particularly useful for highlighting the differences between the dynamics of nonlinear numerical discretizations and the dynamics of the original differential equations, the former often displaying spurious (stable and unstable) fixed points and asymptotes which are not admitted by the latter. It has also been shown [10, 17, 22, 23] how the presence of spurious asymptotes can greatly distort, shrink and/or fragment the basins of attraction of the true solution. (See Yee & Sweby [24, 25] and Griffiths, Sweby & Yee [5] for applications of the dynamics of discretization approach to the study of a range of implicit and explicit Runge-Kutta schemes for a variety of problems.)

The dynamical behaviour of the TVD schemes is dependant upon many things such as the choice of underlying E-scheme, the nonlinear solver used for the implicit schemes (linearization, Newton's method, etc.), and the choice of flux limiter. For the purposes of this report the use of the Engquist-Osher E-scheme, and of linearization to solve the implicit equations, remains constant, with only the effect of the choice of limiter being considered. However, a study of the dynamics of the non-limited (i.e. first order E-O) scheme was made in order to establish the effect of adding a limited numerical flux.

For practical reasons it is necessary to restrict attention to the behaviour of specific points in the scheme, namely the points that lie immediately to the left and right of the shock. This choice is appropriate since experiments indicate that the points in the neighbourhood of the shock are the first to display the instability that leads to non-convergence and residual plateauing. An analysis of the dynamics of these points may therefore give an insight not only into the general behaviour of the schemes, but also into the process of residual plateauing.

The two steady-state shock positions are considered separately. The stable shock at $x = x_1 = 0.18$ and the falsely stable shock at $x = x_2 = 0.82$. In both cases Δx, the space interval, is taken to be $\frac{1}{40}$.

The first step is to assume that all points away from the shock are exact and remain unchanged, giving, in effect, a reduced boundary value problem with two internal points. The point immediately to the left of the shock is denoted X and the point immediately to the right of the shock is denoted Y (see Figure 4.1).

For the stable shock X represents $u_{k=7}$ and Y represents $u_{k=8}$, whereas for the falsely stable shock X represents $u_{k=32}$ and Y represents $u_{k=33}$.

The restriction of the problem to a 2-D system, although being a somewhat artificial description of the full problem, can provide useful information about the influence of the limiters on the dynamics of the scheme. It should be kept in mind, however, when considering the results, that they apply only to this special case.

The fixed points of the first order E-O scheme, both explicit and implicit, can be found analytically and their stability established. Similar analysis for the

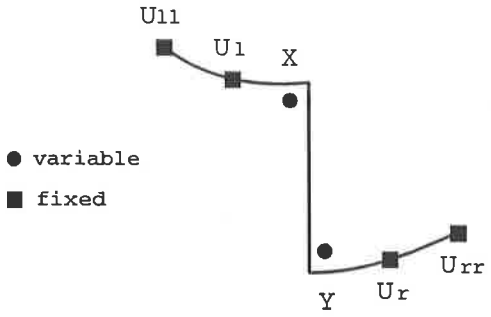

Figure 4.1: Grid points of reduced problem.

TVD schemes is complicated by the use of nonlinear limiters and is best studied using a computational approach. The explicit and implicit formulations of the schemes display quite different dynamical behaviour and are therefore considered separately.

4.1 Explicit Schemes

4.1.1 Fixed Point Analysis of the Reduced E-O Scheme

The full first order explicit Engquist-Osher approximation to the test problem (2.5) is given by

$$u_k^{n+1} = u_k^n - \lambda \left[f_{k+1}^- + f_k^- - f_k^+ - f_{k-1}^+ \right] + \Delta t g(x) u_k^n, \tag{4.1}$$

where $f_k = \frac{1}{2}u_k^2$, $g(x) = 6k\Delta x - 3$, $\Delta x = \frac{1}{40}$ and $f_k^{\pm}$ are as defined for equation (3.3).

For points u_7 and u_8 on the stable shock, with all other points fixed at their exact values, the scheme reduces to the 2-D system

$$\begin{aligned} X^{n+1} &= X^n - \tfrac{\Delta t}{40}\left[f^-(Y^n) + f^-(X^n) - f^+(X^n) - f^+(u_6^n)\right] - \tfrac{39}{20}\Delta t X^n \\ Y^{n+1} &= Y^n - \tfrac{\Delta t}{40}\left[f^-(u_9^n) + f^-(Y^n) - f^+(Y^n) - f^+(X^n)\right] - \tfrac{36}{20}\Delta t Y^n \end{aligned} \tag{4.2}$$

where u_6 and u_9 are known values.

The steady states of this system can be found by setting $X^{n+1} = X^n$ and $Y^{n+1} = Y^n$ and solving for X and Y. Using the definitions of f^+ and f^- to write $f^+(u) = f\left(\frac{1}{2}(u - |u|)\right)$ and $f^-(u) = f\left(\frac{1}{2}(u + |u|)\right)$, and substituting for u_6 and u_9, gives

$$\left.\begin{aligned} -\left(\tfrac{39}{20}\Delta t - 20\Delta t|X^n|\right) X^n - 10\Delta t\left(Y^n - |Y^n|\right) Y^n + 7.628\Delta t &= 0 \\ 10\Delta t\left(X^n + |X^n|\right) X^n - \left(\tfrac{9}{5}\Delta t + 20\Delta t|Y^n|\right) Y^n - 7.764\Delta t &= 0 \end{aligned}\right\} \tag{4.3}$$

There are four cases to consider when solving for X and Y dependant upon their signs.

i) $X^n \geq 0, Y^n \geq 0$. No real fixed points.

ii) $X^n \geq 0, Y^n \leq 0$. Single fixed point at $X^n = 0.36, Y^n = -0.47$.

iii) $X^n \leq 0, Y_n \geq 0$. No real fixed points.

iv) $X^n \leq 0, Y^n \leq 0$. No real fixed points.

Hence there is a single fixed point at $(X^n, Y^n) = (0.36, -0.47)$.

In order to establish the stability of the fixed point it is necessary to examine the eigenvalues of the Jacobian, S, of the 2-D system (4.2). For stability the eigenvalues μ_S must be such that

$$|\mu_S| < 1. \tag{4.4}$$

For the fixed point $(0.36, -0.46)$ the eigenvalues satisfying $|S - \mu_S I| = 0$ are

$$\begin{aligned} \mu_{S1} &= 1 - 34.885\Delta t \\ \mu_{S2} &= 1 - 1.885\Delta t \end{aligned}$$

which satisfy the condition (4.4) for $\Delta t < 0.057$.

So for the first order explicit E-O scheme the stability of the single fixed point at $(X^n, Y^n) = (0.36, -0.47)$ depends explicitly upon the time-step, with the fixed point becoming unstable for $\Delta t \geq 0.057$.

Similar fixed point analysis for points $X = u_{32}$ and $Y = u_{33}$ on the falsely stable shock yields three fixed points, these are

(0.52, 0.26) — stable for $\Delta t < 0.1043$.

(0.40,-0.32) — unstable for all Δt.

(-0.29,-0.53) — stable for $\Delta t < 0.1031$.

4.1.2 Bifurcation Diagrams and Basins of Attraction

The fixed point analysis described previously gives limited information about the dynamics of the reduced numerical system. Fixed points have been located and their stability established but there is no information as to the behaviour of the fixed points when Δt is taken above the stability limit. In addition, analysis was only performed for the non-limited first order scheme since the nonlinear structure of the limited schemes precludes similar investigation. In order to study the dynamics of these schemes it is necessary to turn to computational methods.

The bifurcation diagrams referred to in this section describe the evolution of the fixed points, X and Y, as Δt increases for the various schemes applied to the reduced 2-D problem (4.2). For clarity the fixed points have been split into their X and Y components and displayed on two separate diagrams, although it should be remembered that X and Y are dependant variables. The bifurcation diagrams are produced by first discretizing the variables X, Y and Δt into a $256 \times 256 \times 256$ grid. For each value of Δt, and each initial point (X_0, Y_0) the 2-D system is iterated, typically for around 2000 time-steps, to allow the numerical solution to reach an asymtotic state before the next 10–100 points are plotted.

The basins of attraction diagrams describe the domains of initial points, (X_0, Y_0), which all converge to the same asymptotic state. They are produced in much the same way as the bifurcation diagrams except Δt is kept fixed and

the initial points are colour coded according to where they end up after 2000 iterations. Hence all initial points lying inside a specific shaded region converge to the fixed point contained within that region, represented by a black dot. Unshaded regions represent the domain of initial points which lead to divergence. The basins of attraction diagrams are displayed as plots of X against Y. The dimension of the grid (and hence the accuracy of the diagrams), and the number of initial iterations chosen to allow the solution to settle, are to some degree dependent upon the speed of the computer system being used. The diagrams in this report were produced on a Silicon Graphics Indy R4400 for which the values given above gave acceptable results, although the process is more suited to computation on highly parallel machines such as a Connection Machine.

Figure 4.1.1 shows the X and Y bifurcation diagrams for the fixed points of the 2–D system (4.2), centered on the stable shock, using the explicit E-O scheme. Note that, as predicted by the analysis, there is a single fixed point $(X, Y) = (0.36, -0.47)$ which is stable for $\Delta t < 0.057$. In addition it is now possible to see that for values of Δt greater than 0.057 the fixed point bifurcates, forming period two oscillations in both X and Y. Increase Δt still further and period four oscillations set in. This process continues, lapsing into chaos, before the fixed point disappears completely at around $\Delta t = 0.094$.

The basins of attraction in Figure 4.1.2 illustrate the bifurcation of the fixed point by taking sections in the X-Y plane for a selection of Δt values. Below the stability limit of the scheme the basin covers the whole plane, as instability sets in the basin undergoes a dramatic reduction in size and develops large regions of divergence (represented by areas of no colour).

The explicit flux-limiter schemes, whose bifurcation diagrams and basins of attraction are shown in Figures 4.1.3–4.1.10, display a similar process of period doubling, chaos and reduction in the size of the basin. As with the first order E-O scheme there is a single fixed point (although the position of the fixed point varies from scheme to scheme) and no spurious asymptotic solutions below the linear stability limits of the TVD schemes.

Figures 4.1.11–4.1.20 show the dynamics of the five explicit schemes for the two points, $X = u_{32}$ and $Y = u_{33}$, centred on the unstable shock. Any stable fixed points lying in the bottom right-hand corner of the basin diagrams, corresponding to X being positive and Y negative, would represent convergence to the falsely stable shock solution at $x_2 = 0.82$ of the full problem. Fixed points outside this region have been made stable by the artificial restriction of the problem to a 2-D system, i.e. the fixing of u_{31} and u_{34} to their exact values. Indeed, further analysis of the first order scheme has shown that the introduction of additional 'free' points reduces the stability of these spurious solutions.

The E-O scheme, again in accord with the analysis, possesses two stable fixed points, one at $(0.52, 0.26)$ which is stable for $\Delta t < 0.1043$ and one at $(-0.29, -0.53)$ which is stable for $\Delta t < 0.1031$. The unstable fixed point at $(0.40, -0.32)$ is not picked up in the computation. In this case the basins have begun to shrink before the fixed points have become unstable. Once they do become unstable the basins shrink dramatically and the fixed points quickly lapse into chaos before becoming divergent.

The fixed points of the TVD schemes are much less stable and go through longer periods of bifurcation and chaos. Unlike the first order scheme the pres-

ence of the unstable fixed point can be seen in the dynamics of the four TVD schemes, showing up as a third region of convergence in the basins of attraction diagrams. The appearance of this oscillating solution precipitates a fragmentation and eventual break-up of the basins. This effect is best illustrated in the basin diagrams of the explicit van Leer scheme (Figure 4.1.18).

4.2 Implicit Schemes

4.2.1 Fixed Point Analysis of the Reduced E-O Scheme

As with the explicit formulation of the problem it is possible to use an analytical approach to find the locations and stability of any fixed points of the implicit E-O scheme for the reduced problem. The implicit scheme, applied to the 2–point problem, becomes

$$\boldsymbol{JU} = \boldsymbol{R},$$

where

$$\boldsymbol{J} = \begin{bmatrix} J_{11} & J_{12} \\ J_{21} & J_{22} \end{bmatrix} = \begin{bmatrix} 1+\lambda|X^n| - \Delta t(6x-3) & \frac{\lambda}{2}(Y^n - |Y^n|) \\ -\frac{\lambda}{2}(X^n + |X^n|) & 1+\lambda|Y^n| - \Delta t(6x-3) \end{bmatrix},$$

$$\boldsymbol{U} = \begin{bmatrix} \Delta^- X^{n+1} \\ \Delta^- Y^{n+1} \end{bmatrix} = \begin{bmatrix} X^{n+1} - X^n \\ Y^{n+1} - Y^n \end{bmatrix},$$

$$\boldsymbol{R} = \begin{bmatrix} r_1 \\ r_2 \end{bmatrix}$$

$$= \begin{bmatrix} -\frac{\lambda}{4}[Y^n(Y^n - |Y^n|) + 2X^n|X^n| - u_l(u_l + |u_l|)] + \Delta t(6x-3)X^n \\ -\frac{\lambda}{4}[u_r(u_r - |u_r|) + 2Y^n|Y^n| - X^n(X^n + |X^n|)] + \Delta t(6x-3)Y^n \end{bmatrix},$$

and where $\{u_l, X, Y, u_r\} = \{u_6, u_7, u_8, u_9\}$ or $\{u_{31}, u_{32}, u_{33}, u_{34}\}$ depending on whether the stable or the unstable shock is being considered.

This simple 2×2 system can be solved by inverting the Jacobian matrix J, assuming J is non-singular, to give the recurrance relation

$$\begin{bmatrix} X^{n+1} \\ Y^{n+1} \end{bmatrix} = \frac{1}{J_{11}J_{22} - J_{21}J_{12}} \begin{bmatrix} J_{22} & -J_{12} \\ -J_{21} & J_{11} \end{bmatrix} \begin{bmatrix} r_1 \\ r_2 \end{bmatrix} + \begin{bmatrix} X^n \\ Y^n \end{bmatrix}. \tag{4.5}$$

The fixed points of this system can be found by setting $X^{n+1} = X^n$ and $Y^{n+1} = Y^n$, to give

$$\begin{bmatrix} J_{22}r_1 - J_{12}r_2 \\ J_{11}r_2 - J_{21}r_1 \end{bmatrix} = \begin{bmatrix} 0 \\ 0 \end{bmatrix} \tag{4.6}$$

as necessary conditions on X and Y for a fixed point. By considering the signs of X and Y, and assuming that $J_{11}J_{22} \neq J_{21}J_{12}$, it is straightforward to solve equation (4.6) for X and Y on either of the shocks. Stability is established by checking that the eigenvalues of the system Jacobian, S, are less than one in modulus, where

$$S = \begin{bmatrix} 1 + \frac{d}{dX}\left[\frac{J_{22}r_1 - J_{12}r_2}{J_{11}J_{22} - J_{21}J_{12}}\right] & \frac{d}{dY}\left[\frac{J_{22}r_1 - J_{12}r_2}{J_{11}J_{22} - J_{21}J_{12}}\right] \\ \frac{d}{dX}\left[\frac{J_{11}r_2 - J_{21}r_1}{J_{11}J_{22} - J_{21}J_{12}}\right] & 1 + \frac{d}{dY}\left[\frac{J_{11}r_2 - J_{21}r_1}{J_{11}J_{22} - J_{21}J_{12}}\right] \end{bmatrix}.$$

Calculations show that at the stable shock, $x = x_1 = 0.18$, where $X = u_7$ and $Y = u_8$, there is a single fixed point $(X, Y) = (0.37, -0.48)$ which is stable for all Δt. At the unstable shock, $x = x_2 = 0.82$, where $X = u_{32}$ and $Y = u_{33}$, there are three fixed points $(0.52, 0.26)$, $(-0.29, -0.53)$ and $(0.40, -0.32)$. The first two are stable for all Δt, but the fixed point $(X, Y) = (0.40, -0.32)$ is only stable for $\Delta t > 1.0585$.

4.2.2 Bifurcation Diagrams and basins of attraction

As with the explicit schemes computational methods can be used to provide extra information about the dynamics of the first order scheme, as well as providing descriptions of the behaviour of the nonlinear TVD schemes. The dynamics of the implicit schemes are quite different to that of the explicit schemes. In addition to regions of period doubling and chaos they can also possess spurious steady solutions, even at values of λ below the linear stability limit of the scheme.

At the stable shock position the dynamics of the five implicit schemes are well behaved. The bifurcation diagram of the E-O scheme, mirroring the results given by the analysis, possesses a single fixed point $(X, Y) = (0.37,-0.48)$ which is stable for all Δt. The four TVD schemes all display very similar results with slight differences in the position of the fixed point.

Figures 4.2.1–4.2.10 describe the dynamics of the five implicit schemes at the unstable shock position. All five schemes produce the three fixed points identified in the analysis of the first-order scheme (although the precise position of the fixed points vary from scheme to scheme). As described in Section 4.1.2 fixed points in the region $X > 0, Y < 0$ correspond to convergence to the falsely stable solution of the full problem, indeed the value of Δt at which these fixed points become stable ($\Delta t \approx 1.06$) coincides with the Courant number values given in Table 3.2 marking convergence to the unstable shock. The point $(X_0, Y_0) = (0.52, -0.53)$ represents the initial conditions used in the full problem to represent the shock at x_2.

Figure 4.2.1 shows just such a point occuring at $\Delta t = 1.1$ in the bifurcation diagram of the implicit E-O scheme. The transition from two to three fixed points causes brief periods of chaos and divergence in the lower right-hand quadrant of the basin diagrams in Figure 4.2.2 (analogous to the periods of non-convergence between $c = 11$ and $c = 22$ in the full problem) before the whole quadrant becomes a basin for the new fixed point. (N.B. some of the features shown in the basin of attraction diagrams, such as the brief period of instability in the fixed points when $\Delta t = 0.8$, have been lost in the calculation of the bifurcation diagrams due to computational constraints.)

The dynamics of the TVD schemes (Figures 4.2.3 - 4.2.10) are complicated by the introduction of additional spurious fixed points, causing fragmentation of the basins and a reduction in size of the basin of the falsely stable solution in the lower right-hand quadrant. For the minmod scheme this spurious behaviour, appearing as a Δt dependant period two oscillation, is short lived, allowing the basin to fully recover until it resembles the first-order solution. These spurious fixed points are less evident in the bifurcation diagrams of the implicit van Albada scheme (Figure 4.2.5), appearing only breifly when the falsely stable solution first becomes stable. The effect on the falsely stable solution however is dramatic, causing it to oscillate

chaotically, although the basins appear largely unaffected. The van Leer scheme displays similar dynamics to that of the minmod scheme with the introduction of a spurious period-two oscillating fixed point in the $X > 0, Y < 0$ region. In this case the spurious behaviour persists and the basin of attraction of the falsely stable solution remains greatly reduced (Figure 4.2.8). The superbee scheme is the worst affected with the spurious solutions displaying a higher order of oscillation for a range of Δt. As with the van Leer scheme this behaviour persists causing a severe and lasting reduction in the size of the basin of the falsely stable fixed point.

The results indicate that the more compressive limiters, such as van Leer's and Roe's superbee, suffer more from the effects of spurious solutions introduced by the nonlinear second-order terms. The associated reduction in the size of the basin of attraction of the true (falsely stable) solution increases the chances of the initial conditions leading to spurious oscillations, non-convergence and hence residual plateauing.

5 Residual Plateauing

The results in the previous section highlight the trade-off involved in choosing a particular limiter for a specific problem. Highly compressive limiters, such as superbee and van Leer, produce sharper shock resolution and greater accuracy than more diffusive limiters such as minmod and van Albada. Their drawback is that they have lower stability and slower convergence rates. This is especially true for problems containing strong hypersonic shock waves, see Yee [19, 20]. Even for the 1-D transonic test problem under consideration in this report the instability of the compressive limiters was experienced, causing oscillations around the shocks and leading to the residual plateauing seen in Section 3.

An obvious solution to this problem would be to use less compressive limiters, but since compressive limiters give better results in the majority of cases this solution seems rather drastic. What is needed is an inbuilt mechanism for preventing, or at least curing, the effects of limiter instability.

5.1 Limiter Freezing

Although not placed on any firm theoretical footing the technique of limiter freezing is sometimes employed to provide a 'quick fix' solution to the problem of residual plateauing. The method involves monitoring the residual error in the numerical solution, $|u^{n+1} - u^n|$, until it begins to plateau, then fixing the value of the limiter, i.e. preventing it from being updated at each time-step and thus freezing its value.

One way of monitoring the numerical solution for the onset of instability is to measure the total movement in each of the nodes. Let

$$w_k = w(u_k) = \sum_{m=n_0}^{n} \left| u_k^{m+1} - u_k^m \right|. \tag{5.1}$$

where n_0 is some initial time-step (eg $n = 100$) chosen to allow the scheme time to settle on a solution, and n is the current time-step. The function w_k can be thought of as a 'wobble factor', measuring the total change in the value of the solution at the node u_k. A node which has become unstable and is oscillating will possess a high wobble factor, whereas a node which is stable and remains fixed will have a wobble factor of zero. By setting a threshold value ϵ, above which a node is recognised as being unstable, the wobble factor can be used to trigger limiter freezing.

Naturally not all nodes need to be frozen since most parts of the solution, particularly those points away from the shock, remain stable. Neither is it sufficient to only freeze the limiters at those points lying on the shock, since even small instabilities here can set off instability in neighbouring nodes. By using the wobble factor it is possible to freeze the limiter $\phi(r_k)$ at all points which display a substantial degree of instability, i.e. at points for which $w_k > \epsilon$.

5.2 Results using Limiter Freezing

The method of freezing described above is only suitable for implicit TVD schemes since it causes divergence in the explicit schemes.

Numerical experiments were performed using limiter freezing for the implicit superbee and van Leer limited schemes applied to the scalar test problem (2.5) with an initial jump at the unstable shock position $x = 0.82$. As described in Section 3 these two schemes, under the same conditions, suffered from residual plateauing for certain ranges of Courant number.

The value given to the threshold parameter ϵ was found to be crucial to the effectiveness of the method and dependent upon the choice of limiter. If the value of ϵ was too high then, unless w_k became very large, limiter freezing was never triggered. On the other hand, if the value of ϵ was too low, limiter freezing was triggered prematurely causing the scheme to become unstable. The best results were acheived using a value of $\epsilon = 0.1$ with the superbee limiter (3.5) and $\epsilon = 10^{-5}$ with the van Leer limiter (3.6).

Table 5.1 gives Courant number ranges for convergence to the (physically) stable shock at $x = 0.18$ and the (physically) unstable shock at $x = 0.82$ for the two implicit limiter schemes both with and without limiter freezing.

scheme	converges to x_1	converges to x_2
superbee	$c < 11$	—
frozen superbee	$c < 11$	$22 < c < 55$
van Leer	—	—
frozen van Leer	$c < 11$	$c > 22$

Table 5.1: Convergence regions for frozen & non-frozen schemes.

For $c < 11$ both schemes converged to the stable steady solution with a shock at $x = 0.18$. In the case of the superbee limiter the scheme was already convergent within this range and indeed limiter freezing was not activated. The van Leer scheme however did benefit from limiter freezing and converged for values of $c < 11$ at which it previously suffered from residual plateauing. Limiter freezing also had the side-effect of causing the van Leer scheme to converge to the falsely stable steady solution for values of $c > 22$, as shown in Figure 5.1 for $c = 300$.

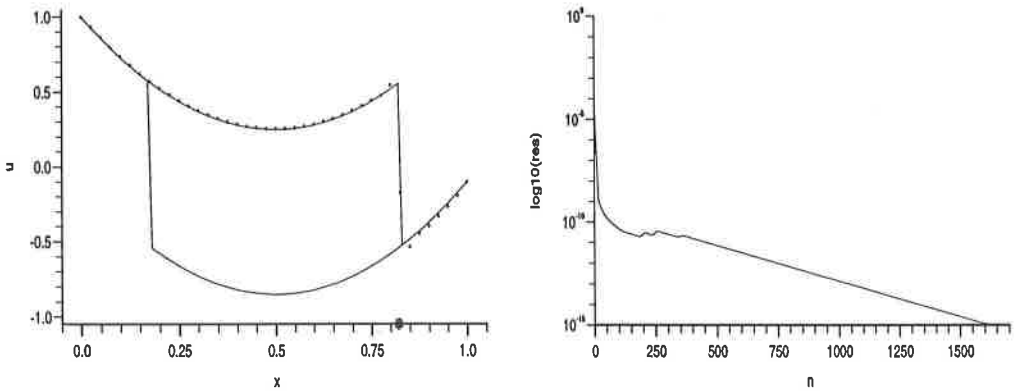

Figure 5.1: Implicit van Leer TVD scheme with limiter freezing, c=300

This stabilising of the physically unstable steady solution was experienced to a lesser degree by the frozen superbee scheme. Although the scheme converged for $22 < c < 55$ residual plateauing still occured for Courant numbers in the

range $55 \leq c \leq 130$, after which the scheme became convergent once more. As c was increased past $c = 160$ the solution jumped suddenly from the falsely stable steady solution with a shock at $x = 0.82$ (Figure 5.2) to a completely spurious non-physical solution (Figure 5.3). This solution persisted until plateauing returned for $180 < c < 260$. For $c \geq 260$ the scheme converged to a non-physical solution containing a shock at the right boundary caused by the fixed boundary value (Figure 5.4).

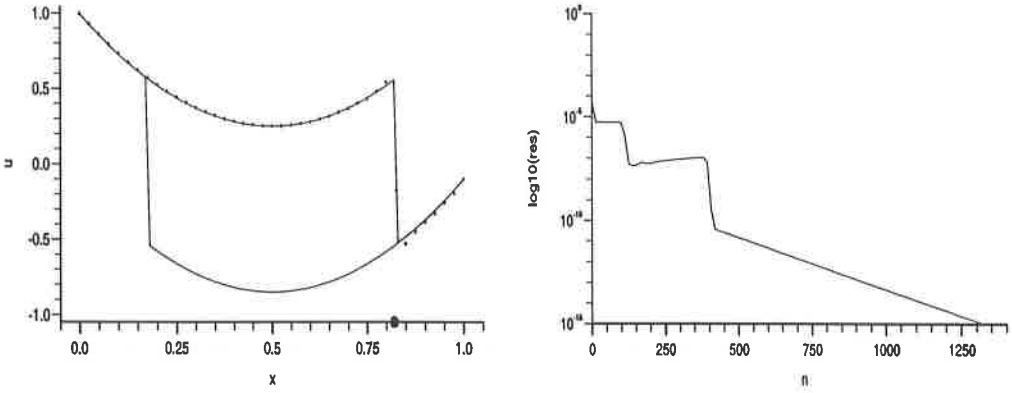

Figure 5.2: Implicit superbee TVD scheme with limiter freezing, c=150

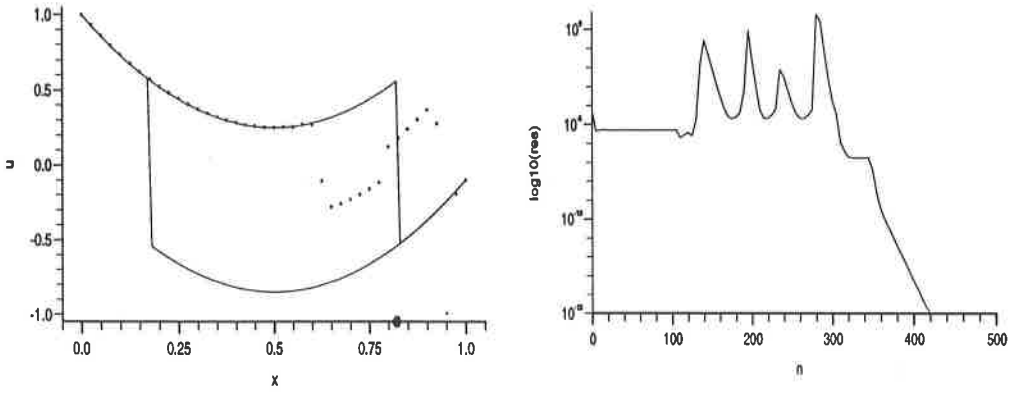

Figure 5.3: Implicit superbee TVD scheme with limiter freezing, c=160

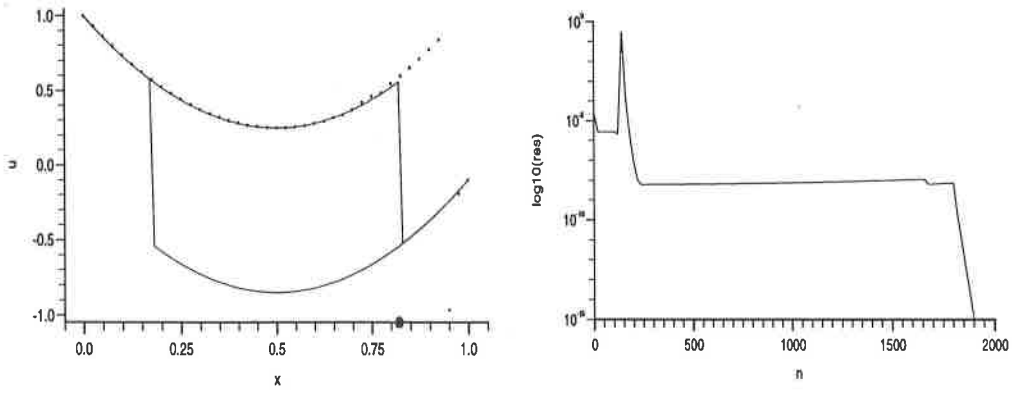

Figure 5.4: Implicit superbee TVD scheme with limiter freezing, c=300

It is clear from these results that the method of limiter freezing described in Section 5.1, whilst reducing the effects of residual plateauing, does so at the cost of introducing spurious solutions. A bifurcation analysis of the frozen schemes applied to the reduced 2-D problem of Section 4 clearly shows the extent to which the dynamics of the schemes have been affected by the introduction of limiter freezing (Figures 5.2.1 & 5.2.2).

The addition of a host of closely packed spurious fixed points greatly reduces the chances of converging to the true solution. The basins of attraction in Figures 5.2.3 and 5.2.4 have become fragmented, severely so in the case of the superbee limiter, making the numerical solution highly dependent on both the time-step Δt and the initial conditions. This effect can be seen in the full problem by comparing the solutions given in Figures 5.2 and 5.5. Both graphs show converged solutions for the frozen superbee limiter scheme with Courant number $c = 150$. In Figure 5.2 initial conditions have been chosen with a shock at $x = 0.82$ whereas in Figure 5.5 the initial conditions contained a shock at $x = 0.916$. The two solutions differ significantly.

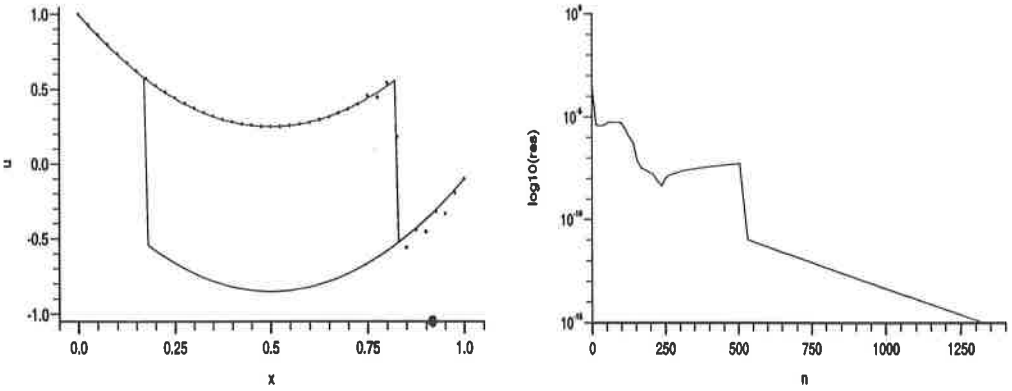

Figure 5.5: Implicit superbee TVD scheme with limiter freezing, c=150.

The high dependence on initial values and the untrustworthiness of the solutions make limiter freezing an extremely unreliable method. This is perhaps not surprising since it relies on switching off the solution monitoring mechanism that makes TVD schemes so desirable. A method is needed that will encourage convergence whilst preserving the properties of TVD.

5.3 Limiter Switching

An alternative solution to the problem of residual plateauing is that of limiter switching which combines the advantages of the highly compressive, yet less stable, limiters and the more stable, less compressive limiters. The idea is to use a highly compressive limiter wherever possible, switching to a less compressive limiter for points displaying signs of instability. This can be done using the 'wobble factor' w_k, defined by equation (5.1), to detect oscillations in the numerical solution at each grid point. If w_k grows large enough to exceed some predetermined threshold value, ϵ, then the method switches to a more stable limiter at that grid point for all subsequent time-steps. The solution obtained through this method is therefore a hybrid of the two limiters. The advantage of this method over that

of limiter freezing is that it maintains the TVD structure, using a nonlinear flux limiter to adapt the scheme according to the current solution.

5.4 Results using Limiter Switching

The method of limiter switching was tested on the scalar test problem (2.5) using superbee and van Leer as the initial high-compression limiters switching to either minmod or van Albada if the scheme became unstable. Table 5.2 describes the convergence behaviour of the implicit limiter-switching schemes for the various combinations of limiter, with initial conditions possessing an initial shock at $x = 0.82$, the unstable shock position. These values can be compared with those given in Table 3.2 for the straight superbee and van Leer schemes.

scheme	converges to x_1	converges to x_2
superbee-minmod	$c < 11$	$22 < c < 57$ $122 < c < 174$ $c > 295$
superbee-van Albada	$c < 11$	$22 < c < 103$ $c > 309$
van Leer-minmod	$c < 11$	$c > 22$
van Leer-van Albada	$c < 11$	$c > 22$

Table 5.2: Comparison of convergence regions for limiter-switching schemes.

As with the limiter-freezing method limiter-switching improves the general convergence of the problem irrespective of whether it is to the stable or unstable solution. Whereas the straight superbee scheme only converged for $c < 11$ both of the superbee schemes with limiter-switching also demonstrate convergence for ranges of Courant number greater than $c = 22$. The superbee scheme with minmod switching is perhaps more successful than the scheme with van Albada switching in this respect since it converges for a wider range of Courant number, even though it possesses more regions of non-convergence. Unlike the situation with limiter-freezing, where each range of Courant number represented convergence to a different solution, the solutions gained from limiter-switching (for $c > 22$) are independent of the value of c. Figures 5.6 and 5.7 show the solutions obtained from the two superbee limiter-switching schemes for $c = 310$.

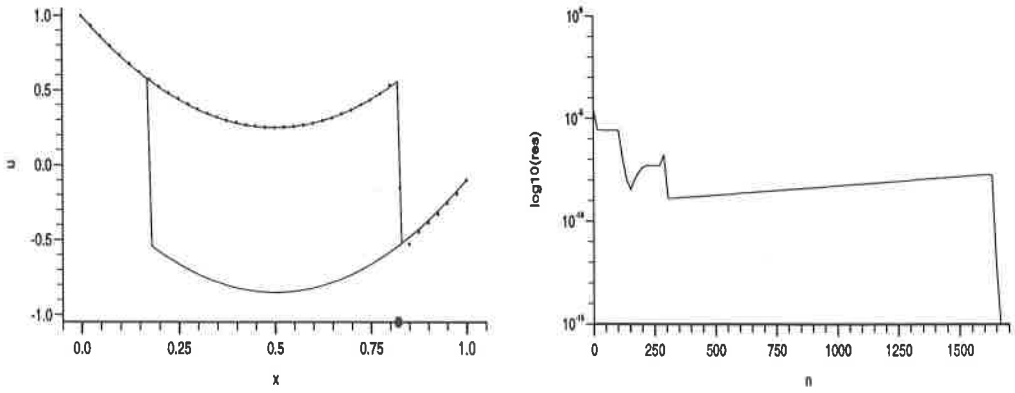

Figure 5.6: Implicit superbee scheme with minmod switching, c=310.

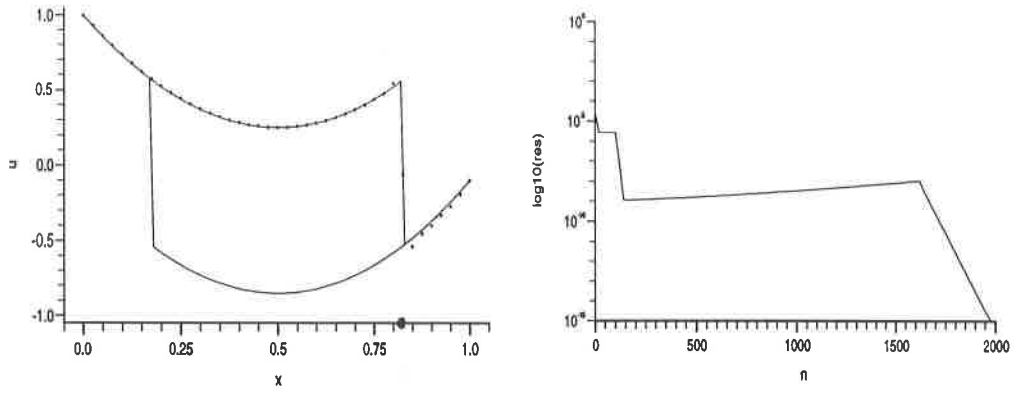

Figure 5.7: Implicit superbee scheme with van Albada switching, c=310.

The two limiter-switching van Leer schemes show a marked improvement over the straight van Leer scheme in terms of convergence. Whereas the straight van Leer scheme did not converge for any value of c (Table 3.2) both of the switching schemes demonstrate convergence for the same Courant number ranges as the underlying E-O scheme. The scheme using van Albada switching has a slight advantage in that it tends to converge slightly faster, as shown in Figures 5.8 and 5.9.

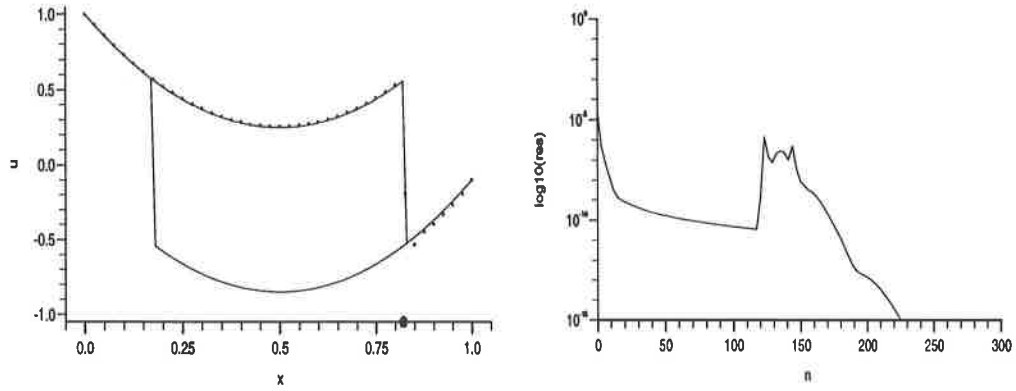

Figure 5.8: Implicit van Leer scheme with minmod switching, c=310.

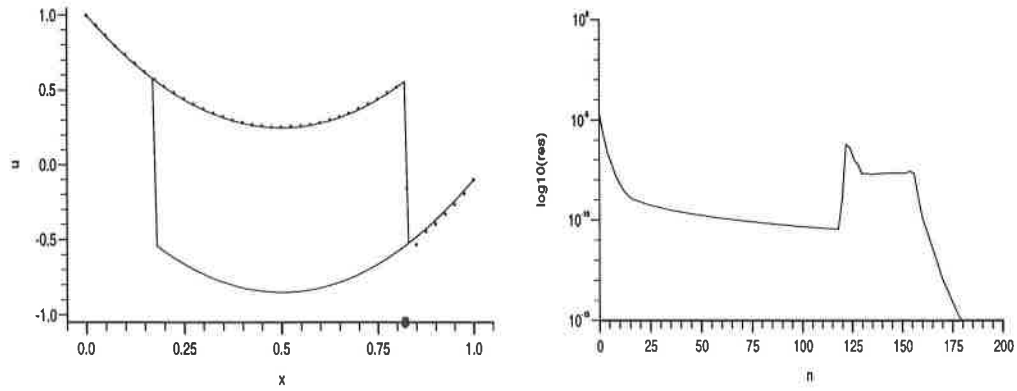

Figure 5.9: Implicit van Leer scheme with van Albada switching, c=310.

The effect of limiter switching on the dynamics of the reduced problem is clearly illustrated in the bifurcation diagrams of the superbee-minmod and van Leer-minmod schemes in Figures 5.3.1 and 5.3.2. Whereas the stable solutions of the primary limiters (i.e. superbee and van Leer) remain intact the spurious oscillating solutions are replaced by the dynamics of the switching (minmod) limiter. The persistant spurious fixed points of the superbee and van Leer schemes are therefore replaced by the short-lived spurious behaviour of the minmod scheme.

Figures 5.3.3 and 5.3.4 show the basins of attraction of the two limiter-switching schemes for $\Delta t = 40$, long after the spurious behaviour of the minmod scheme has died off. In Figure 5.3.3 the region $X > 0, Y < 0$ is composed of two basins of attraction, with one set of initial conditions converging to the falsely-stable fixed-point solution of the superbee scheme and the other converging to the (nearby) falsely-stable fixed-point solution of the minmod limiter.

Although the limiter-switching schemes retain the same basic dynamical structure as the primary limiter the introduction of a well-behaved switching limiter appears to lessen the effect of, or even completely remove, the influence of spurious asymptotic solutions arising from the limited anti-diffusive flux terms. In the full problem therefore, at values of Δt for which the superbee and van Leer schemes suffered residual plateauing, their solutions are replaced by those of the well-behaved minmod scheme. It is this feature which leads to the increased stability and improved convergence capabilities of the limiter-switching schemes.

6 Concluding Remarks

Explicit and implicit formulations of an E-O upwind based TVD scheme, using a selection of flux limiters, were used to approximate the solution of a scalar transonic flow problem possessing multiple steady-states. It was shown how an implicit discretization of the problem can result in a physically unstable solution of the original ODE becoming a stable solution of its numerical counterpart.

The problem was reduced to a 2-D system in order to allow a study of the dynamics of the numerical solution at points on the stable and unstable shocks. The explicit schemes were shown to possess no spurious dynamics below their respective stability limits. As Δt was increased above the stability limit the schemes entered a period of bifurcation and chaos accompanied by a dramatic shrinkage in the numerical basins of attraction.

The dynamics of the implicit schemes at the unstable shock showed the falsely stable fixed point becoming stable for sufficiently large values of Δt. For all the limiters tested the stabilizing of the fixed point was accompanied by the introduction of additional, spurious fixed points. These spurious solutions caused fragmentation, and a reduction in size, of the basin of the falsely stable fixed point. The fact that the more compressive limiters exhibited greater disruption of the numerical basins due to the effects of the spurious fixed points seems a likely cause of the phenomenon of residual plateauing experienced in the full problem.

Two methods for combatting residual plateauing were studied. Although improving convergence rates limiter-freezing, whereby the value of the limiter is kept from being updated at points exhibiting instability, did so at the cost of introducing a great number of spurious fixed points, causing a severe fragmentation of the numerical basin of attraction and leading to multiple spurious solutions with a high dependence on initial conditions. The method of limiter-switching on the other hand, which switches to a less compressive, more stable limiter at points exhibiting instability, replaced the spurious behaviour of the primary limiter with the more stable behaviour of the switching limiter. This lead to improved basins of attraction and convergence rates. Although the resolution of the solution at certain points in the full problem (notably points around the shock) was only as good as allowed by the less compressive limiter, limiter-switching was only enabled for values of Δt for which the more compressive limiter would have caused non-convergence. For other values of Δt the resolution remained as for the more compressive limiter.

It is important to note that both methods enhanced convergence to the steady solutions of the underlying E-scheme irrespective of the physical stability of these solutions. In particular, whilst the limiter-switching method reduced the influence of spurious fixed points introduced by the limited anti-diffusive flux terms, and improved convergence to the true solution with a shock at $x = 0.18$, it also increased the stability of the falsely stable solution at $x = 0.82$. Clearly other techniques are needed to identify and account for such falsely stable solutions.

References

[1] S.R. Chakravarthy & S. Osher, *A new class of high accuracy TVD schemes for hyperbolic conservation laws.*
AIAA Paper No. 85–0363, 1985.

[2] B. Engquist & S. Osher, *Stable and entropy satisfying approximations for transonic flow calculations.*
Math. Comp. 34, pp 45–75, 1980.

[3] B. Engquist & S. Osher, *One-sided difference approximations for nonlinear conservation laws.*
Math. Comp. 36, pp 321–351, 1981.

[4] P. Embid, J. Goodman & A. Majda, *Multiple steady states for 1-D transonic flow.*
SIAM J. Sci. Stat. Comput. 5, No.1, 1984.

[5] D.F. Griffiths, P.K. Sweby & H.C. Yee, *On spurious asymptotic numerical solutions of explicit Runge-Kutta methods.*
IMA J. Num. Anal. 12, pp 319-338, 1992.

[6] A. Harten, *High resolution schemes for hyperbolic conservation laws.*
J. Comp. Phys. 49, pp 357–393, 1983.

[7] A. Harten, *On a class of high resolution total variation stable finite difference schemes.*
SIAM J. Num. Anal. 21, pp 1–23, 1984.

[8] C. Hirsch, *Numerical computation of internal and external flows.*
John Wiley & Sons, 1990.

[9] A. Iserles, *Stability and dynamics of numerical methods for nonlinear ordinary differential equations.*
IMA J. Num. Anal. 10, pp 1–30, 1990.

[10] A. Iserles, A.T. Peplow & A.M. Stuart, *A unified approach to spurious solutions introduced by time discretization. Part I: Basic theory.*
SIAM J. Num. Anal. 28, No.6, pg 1723, 1991.

[11] R.J. LeVeque, *Numerical methods for conservation laws.*
Birkhauser, 1990.

[12] R.J. LeVeque, & H.C. Yee, *A study of numerical methods for hyperbolic conservation laws with stiff source terms.*
J. Comp. Phys. 86, pp 187–210, 1990.

[13] S. Osher, *Riemann solvers, the entropy condition, and difference approximations.*
SIAM J. Num. Anal. 21, pp 217–235, 1984.

[14] P.L. Roe, *Generalized formulation of TVD Lax-Wendroff schemes.*
ICASE Report 84–53 NASA CR–172478, NASA Ames Research Center, 1984.

[15] P.K. Sweby, *High resolution schemes using flux limiters for hyperbolic conservation laws.*
SIAM J. Num. Anal. 21, pp 995–1011, 1984.

[16] P.K. Sweby, *TVD schemes for inhomogeneous conservation laws.*
Proc. Nonlinear Hyperbolic Equations – Theory, Computation, Methods and Applications, Eds. J. Ballmann & R. Jeltsch, Notes on Numerical Fluid Mechanics 24, Vieweg, pp 599–607, 1988.

[17] P.K. Sweby & H.C. Yee, *On spurious asymptotic numerical solutions of* 2×2 *systems of ODE's.*
Numerical analysis report 7/91, University of Reading, England.

[18] E. Tadmor, *Numerical viscocity and the entropy condition for conservative difference schemes.*
Math. Comp. 43, pp 369–381, 1984.

[19] H.C. Yee, *Construction of explicit and implicit symmetric TVD schemes and their applications.*
J. Comp. Phys. 68, pp 151–179, 1987.

[20] H.C. Yee, *A class of high-resolution explicit and implicit shock-capturing methods.*
NASA TM–101088, NASA Ames Research Center, 1989.

[21] H.C. Yee, G.H. Klopfer & J.-L. Montague, *High-resolution shock-capturing schemes for inviscid and viscous hypersonic flows.*
J. Comp. Phys. 88, pp 31–61, 1990.

[22] H.C. Yee, P.K. Sweby & D.F. Griffiths, *Dynamical approach study of spurious steady-state numerical solutions of nonlinear differential equations I. The dynamics of time discretization and its implications for algorithm development in computational fluid dynamics.*
J. Comp. Phys. 97, No.2, pp 249–310, 1991.

[23] H.C. Yee, & P.K. Sweby, *Dynamical approach study of spurious steady-state numerical solutions of nonlinear differential equations II. The dynamics of numerics of systems of* 2×2 *ODEs and its connection to finite discretizations of nonlinear PDEs.*
NASA RNR–92–008, NASA Ames Research Center, 1992.
To appear in Int. J. CFD.

[24] H.C. Yee, & P.K. Sweby, *Global asymptotic behaviour of iterative implicit schemes.*
International Journal of Bifurcation & Chaos 4, No.6, pp 1579–1611, 1994

[25] H.C. Yee, & P.K. Sweby, *The dynamics of some iterative implicit schemes.*
Contemporary Mathematics 172, 1994.

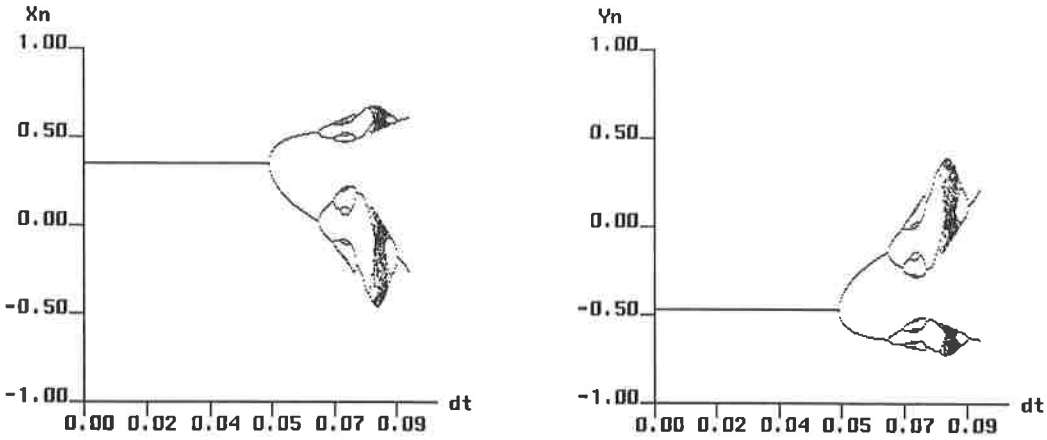

Figure 4.1.1 : Bifurcation diagrams for fixed points at the stable shock. 1st order explicit E-O scheme.

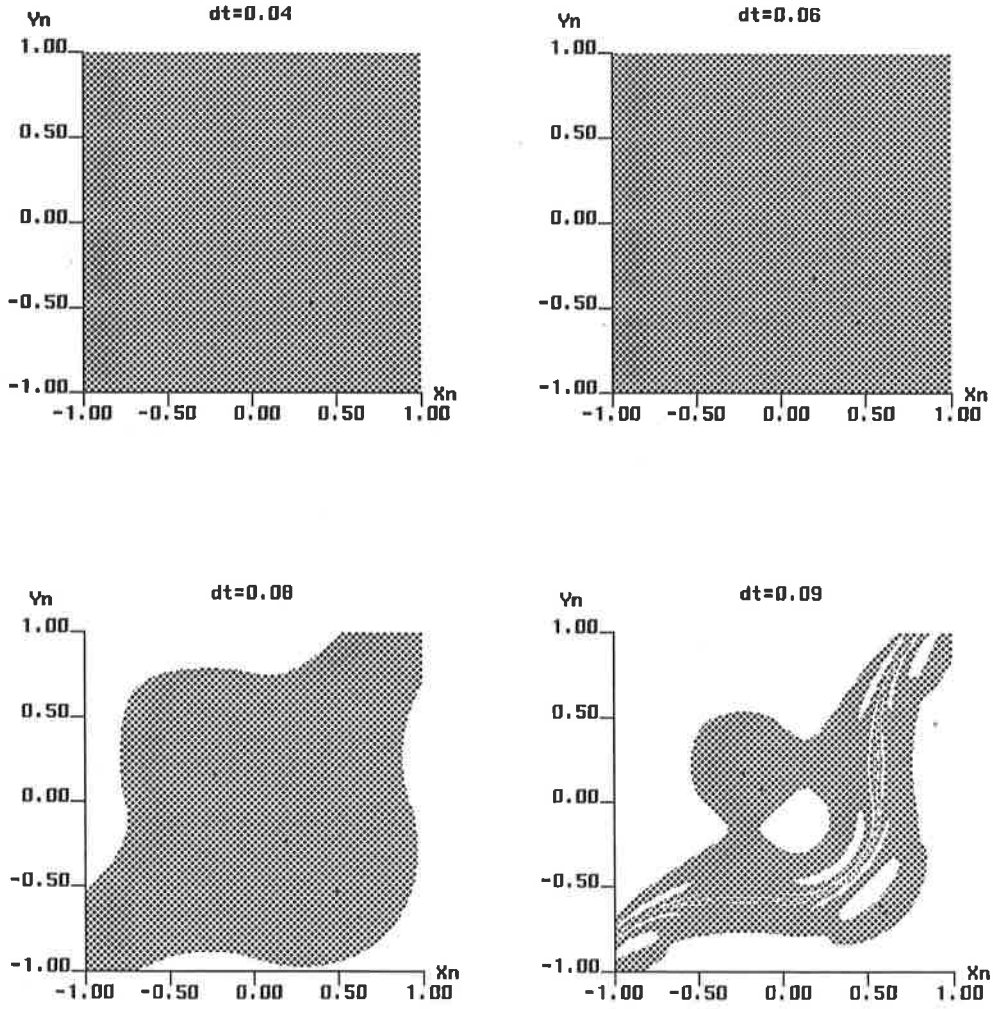

Figure 4.1.2 : Basins for fixed points at the stable shock. Explicit E-O scheme.

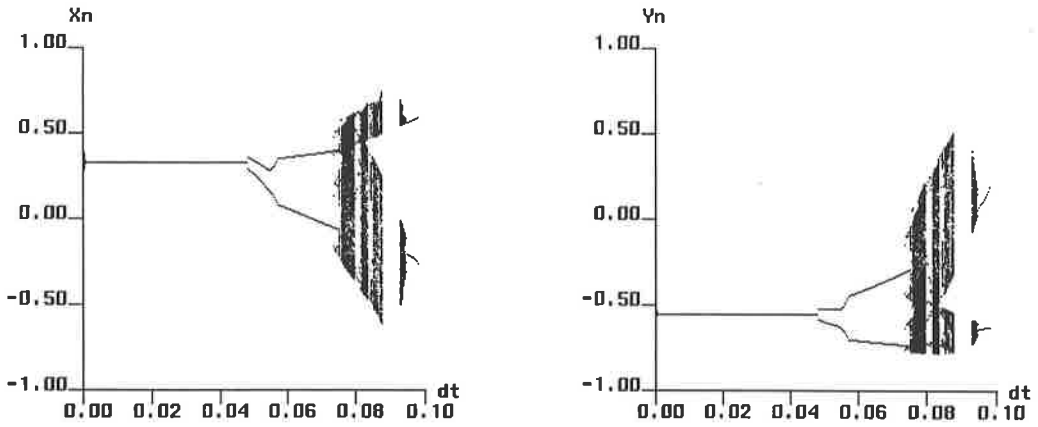

Figure 4.1.3 : Bifurcation diagrams for fixed points at the stable shock. Explicit minmod TVD scheme.

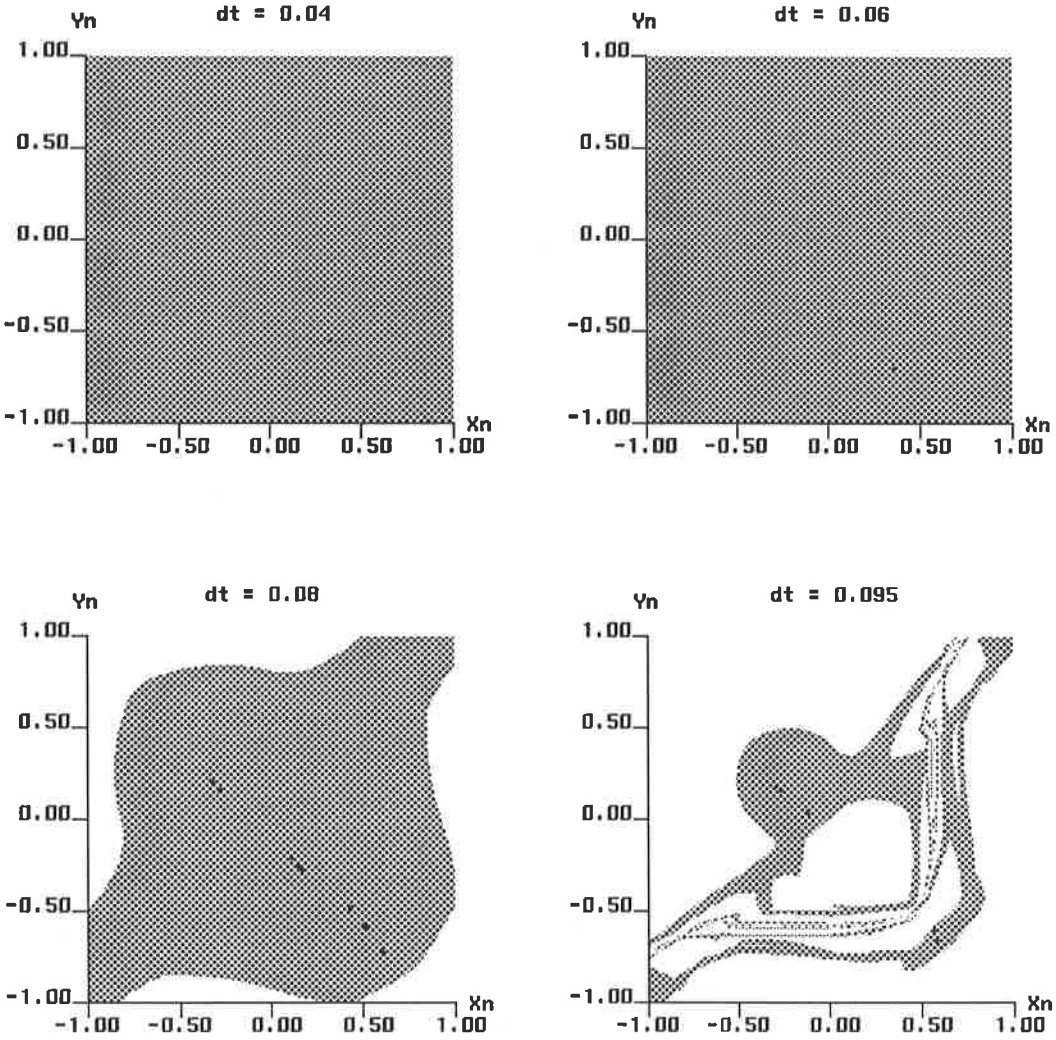

Figure 4.1.4 : Basins for fixed points at the stable shock. Explicit minmod TVD scheme.

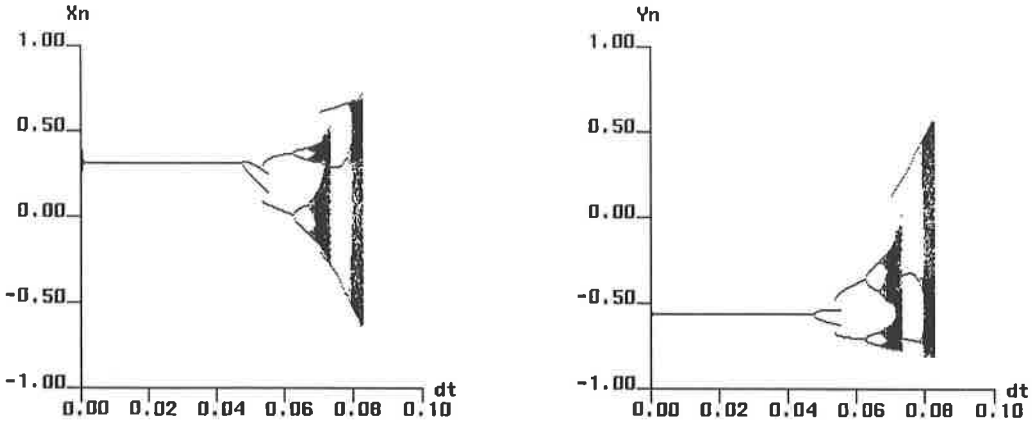

Figure 4.1.5 : Bifurcation diagrams for fixed points at the stable shock. Explicit van Albada TVD scheme.

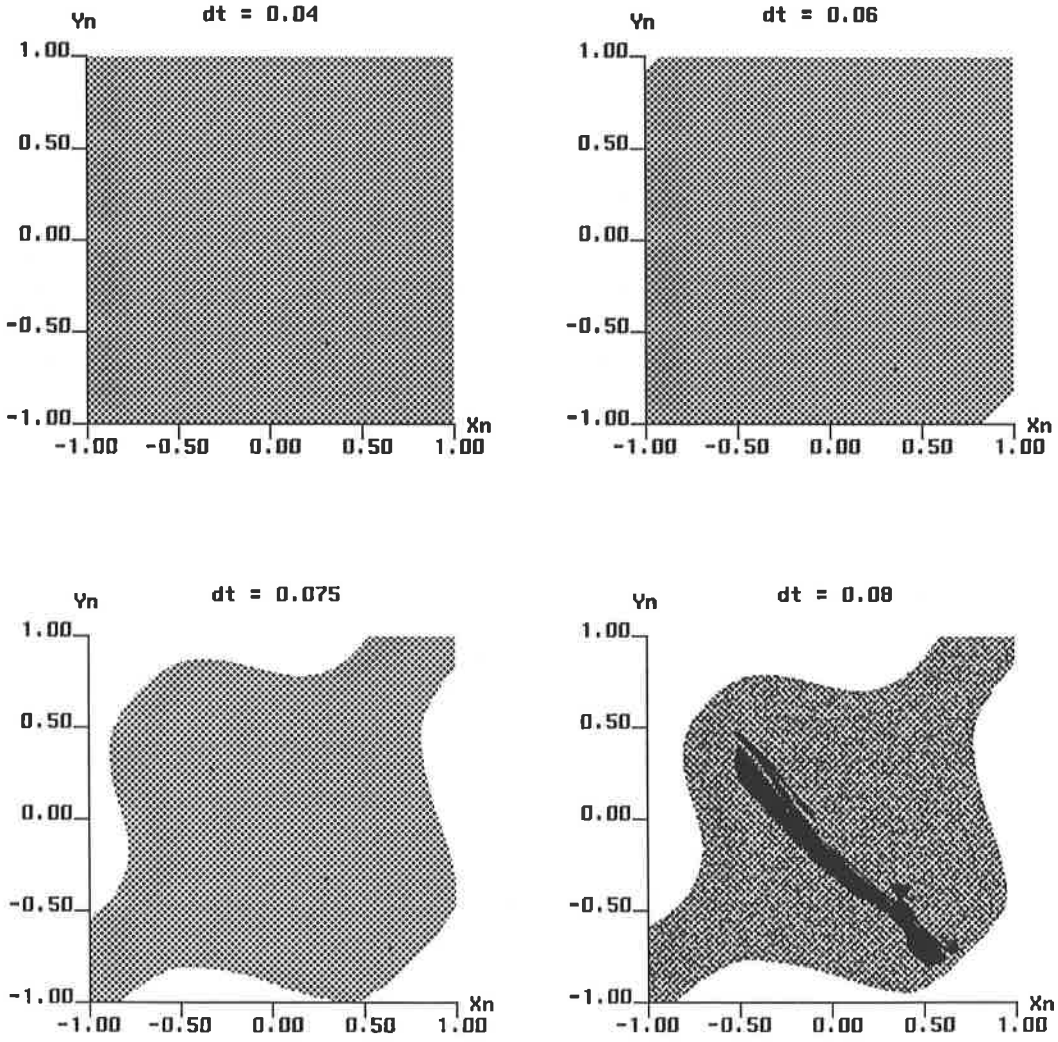

Figure 4.1.6 : Basins for fixed points at the stable shock. Explicit van Albada TVD scheme.

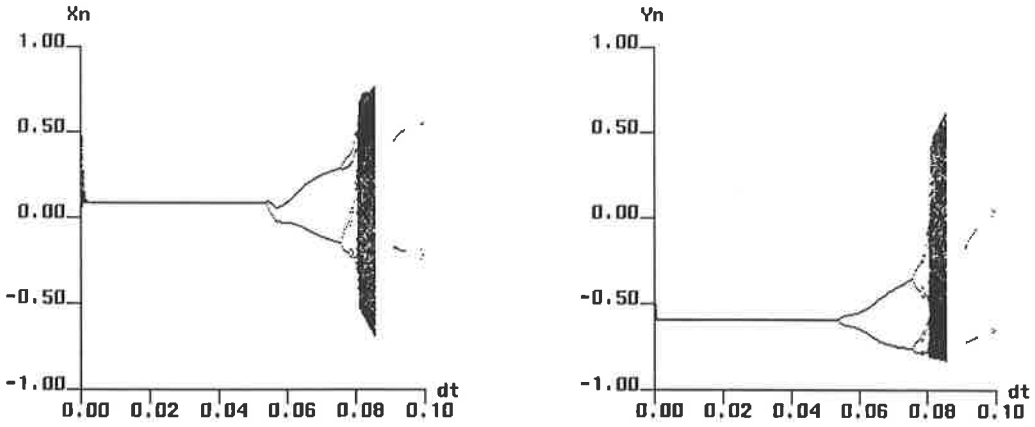

Figure 4.1.7 : Bifurcation diagrams for fixed points at the stable shock. Explicit van Leer TVD scheme.

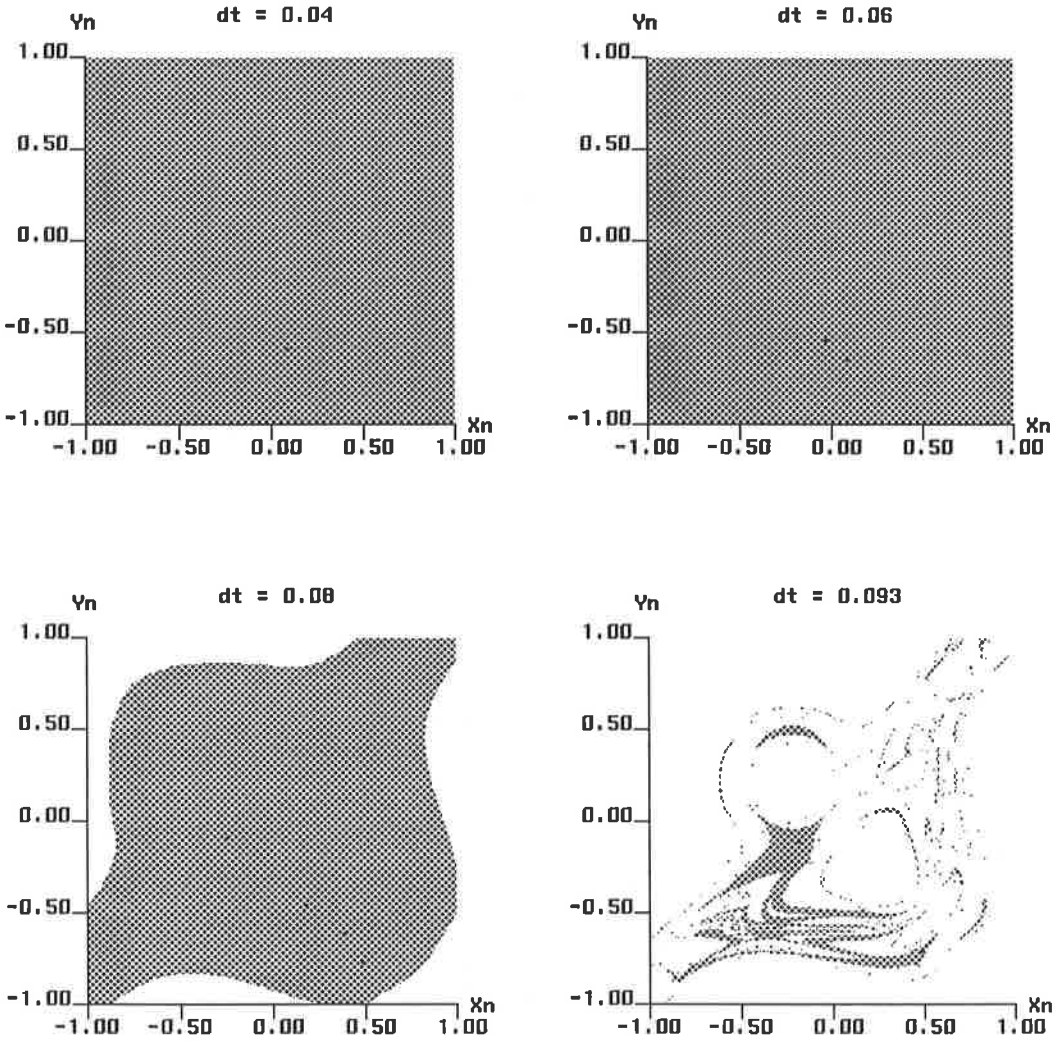

Figure 4.1.8 : Basins for fixed points at the stable shock. Explicit van Leer TVD scheme.

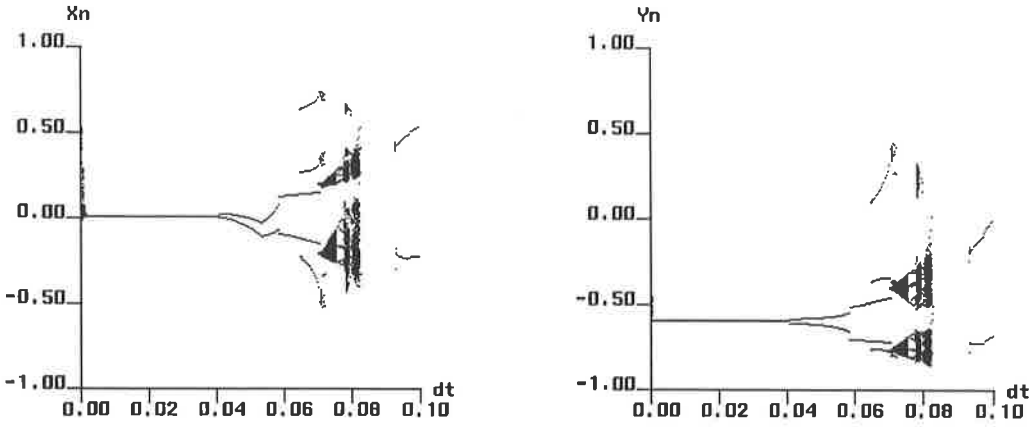

Figure 4.1.9 : Bifurcation diagrams for fixed points at the stable shock. Explicit superbee TVD scheme.

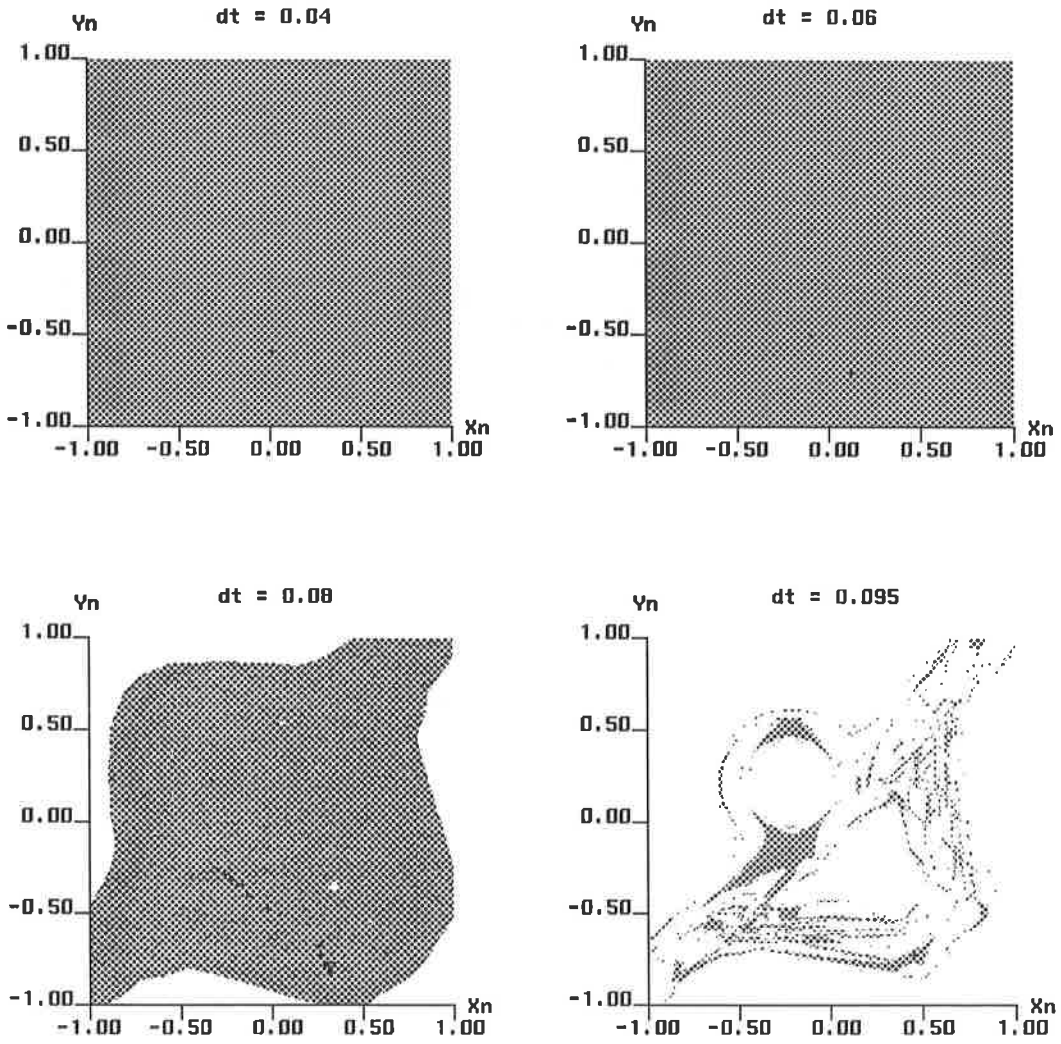

Figure 4.1.10 : Basins for fixed points at the stable shock. Explicit superbee TVD scheme.

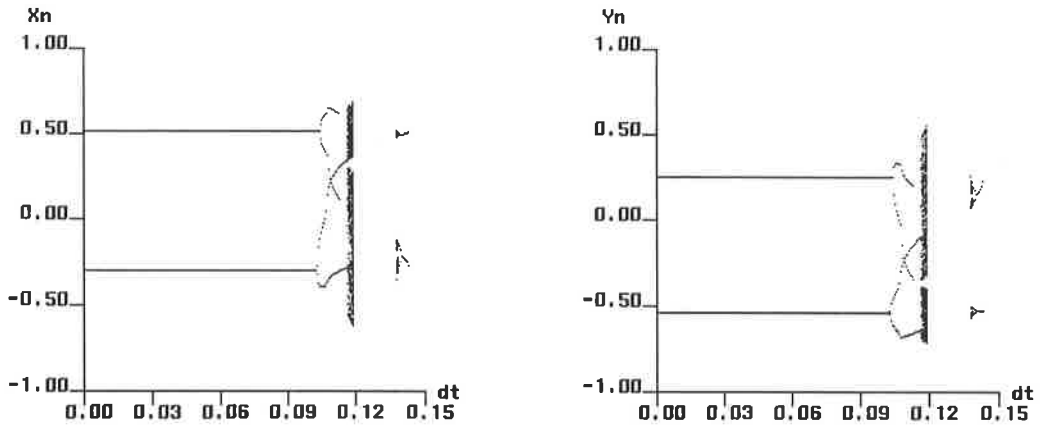

Figure 4.1.11 : Bifurcation diagrams for fixed points at the unstable shock. 1st order explicit E-O scheme.

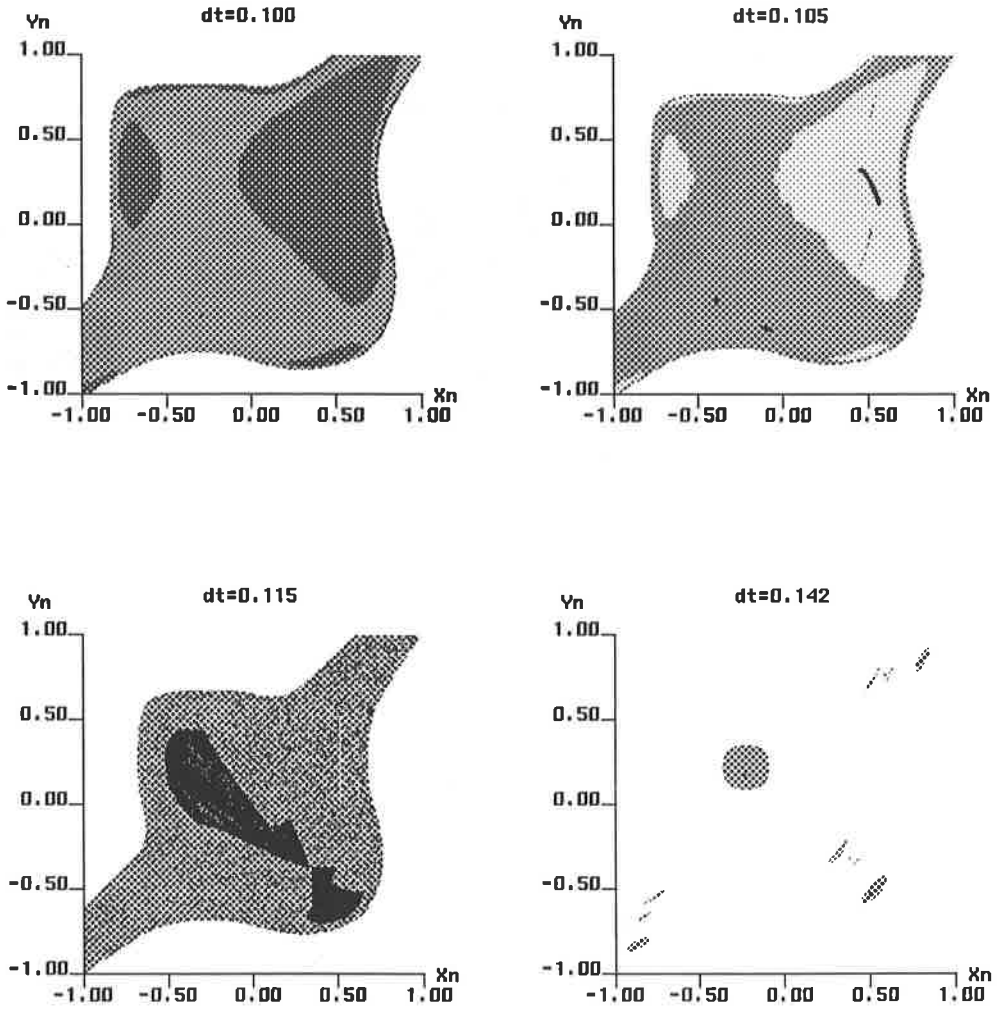

Figure 4.1.12 : Basins for fixed points at the unstable shock. Explicit E-O scheme.

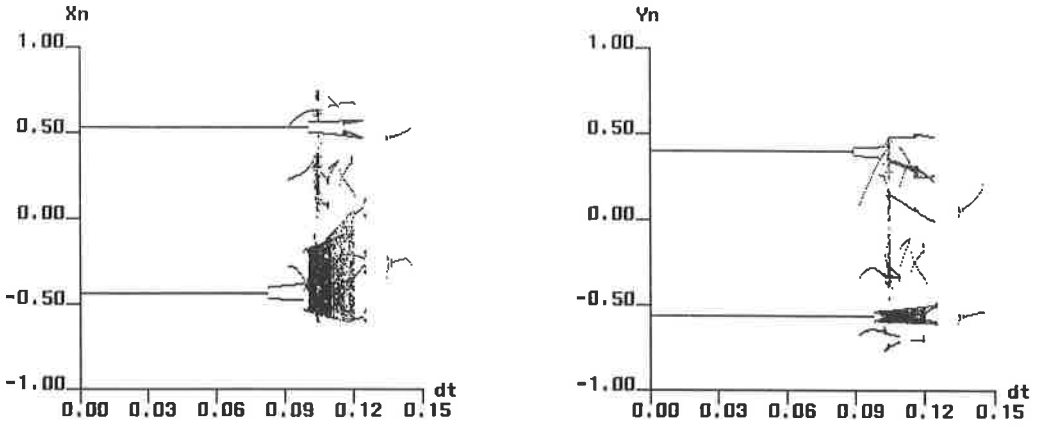

Figure 4.1.13 : Bifurcation diagrams for fixed points at the unstable shock. Explicit minmod TVD scheme.

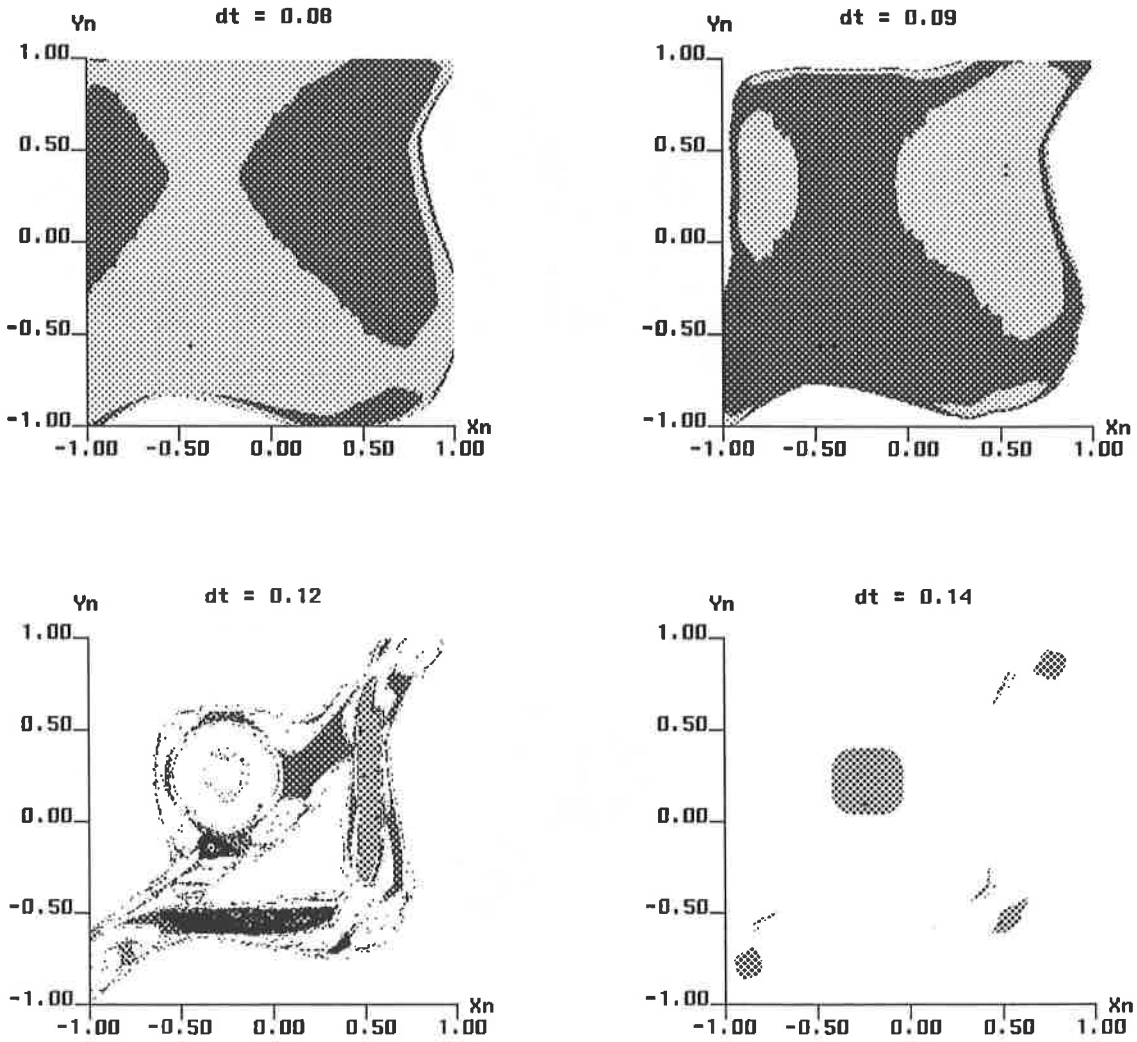

Figure 4.1.14 : Basins for fixed points at the unstable shock. Explicit minmod TVD scheme.

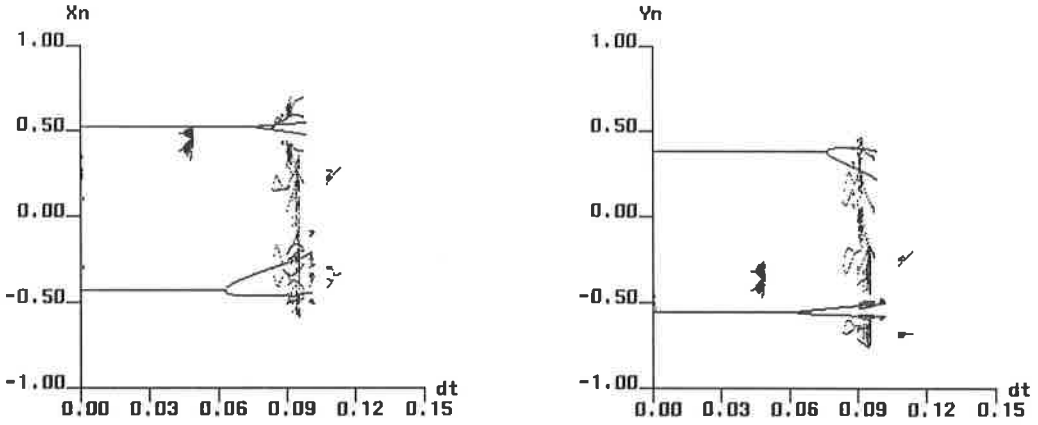

Figure 4.1.15 : Bifurcation diagrams for fixed points at the unstable shock. Explicit van Albada TVD scheme.

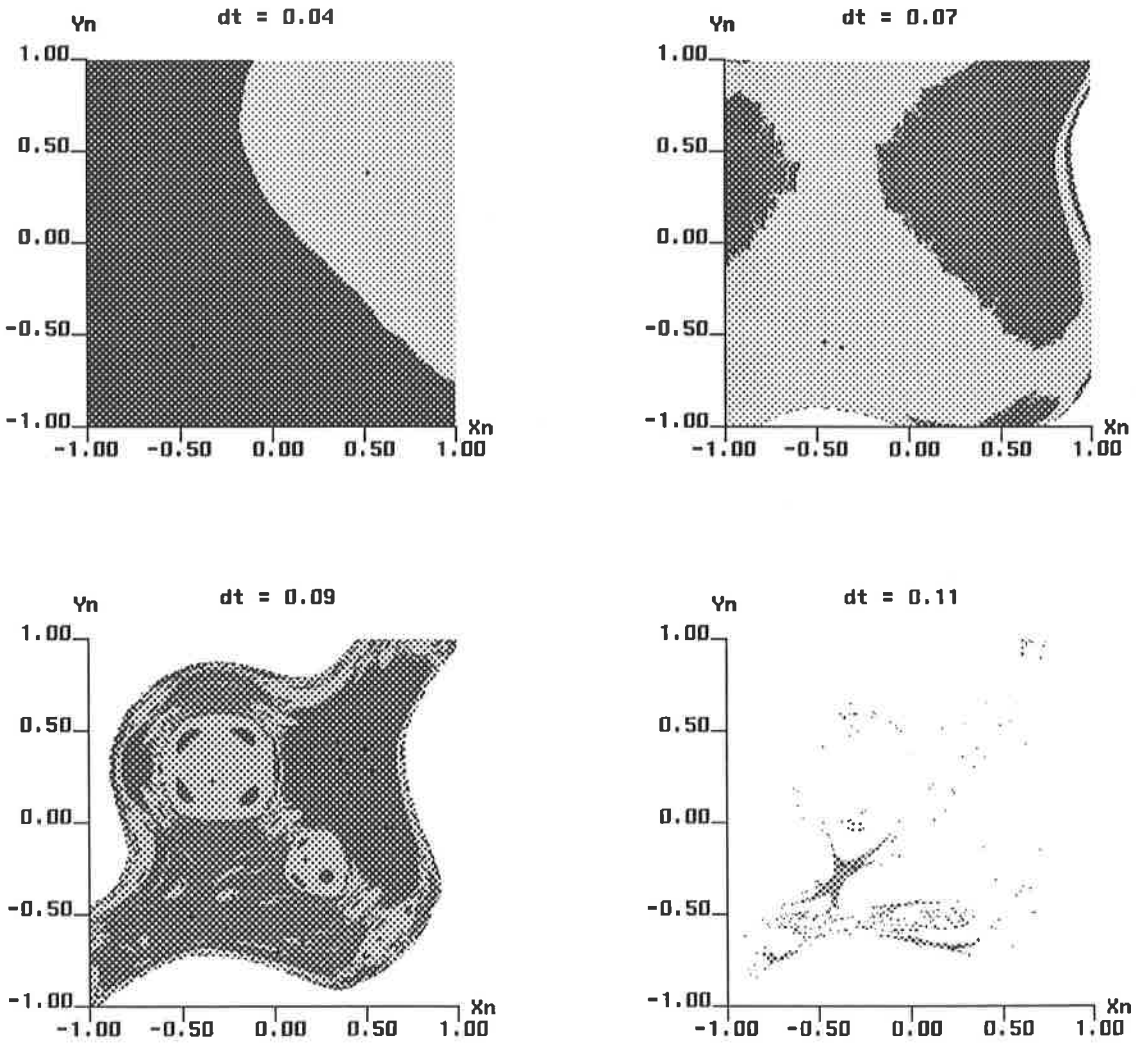

Figure 4.1.16 : Basins for fixed points at the unstable shock. Explicit van Albada TVD scheme.

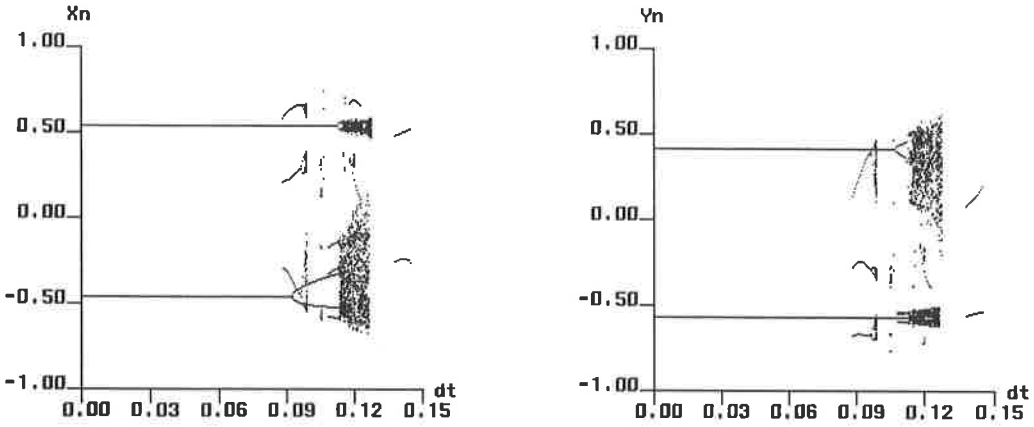

Figure 4.1.17 : Bifurcation diagrams for fixed points at the unstable shock. Explicit van Leer TVD scheme.

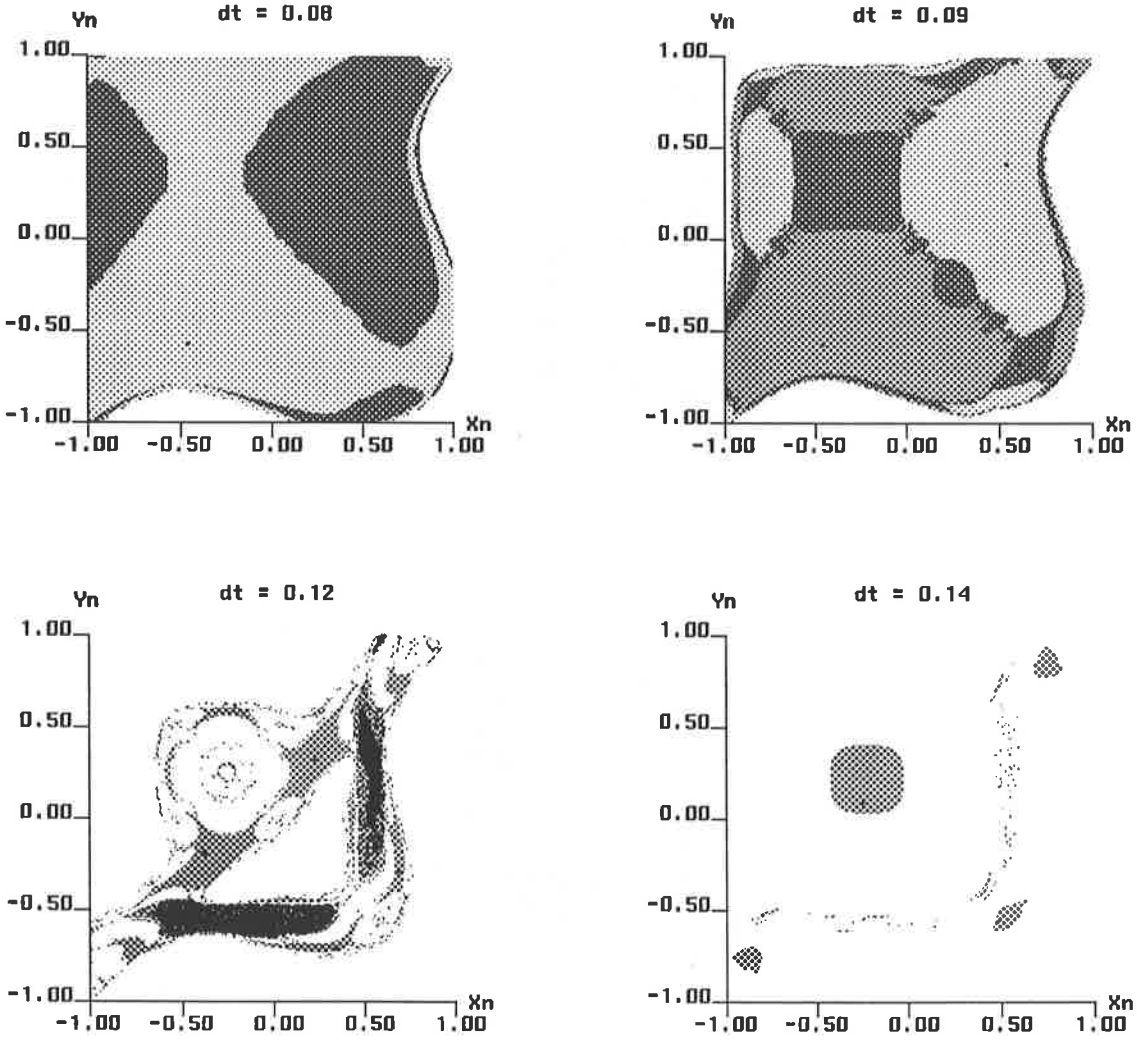

Figure 4.1.18 : Basins for fixed points at the unstable shock. Explicit van Leer TVD scheme.

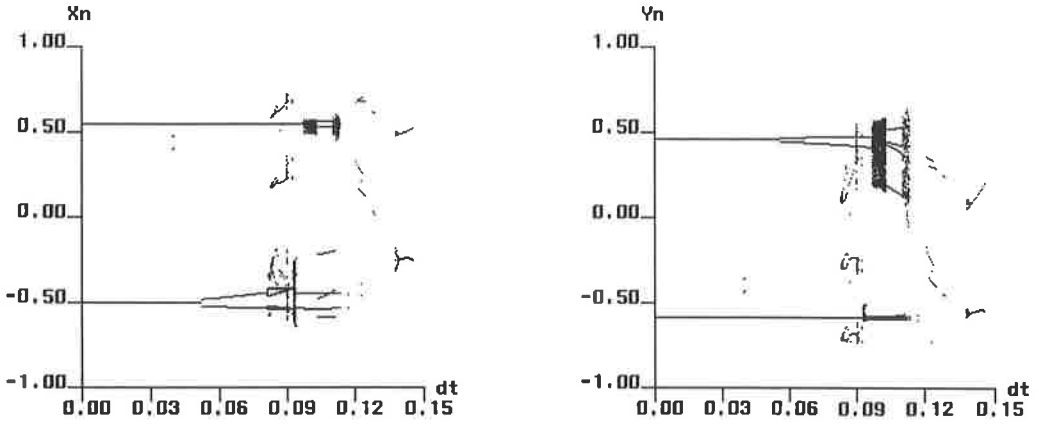

Figure 4.1.19 : Bifurcation diagrams for fixed points at the unstable shock. Explicit superbee TVD scheme.

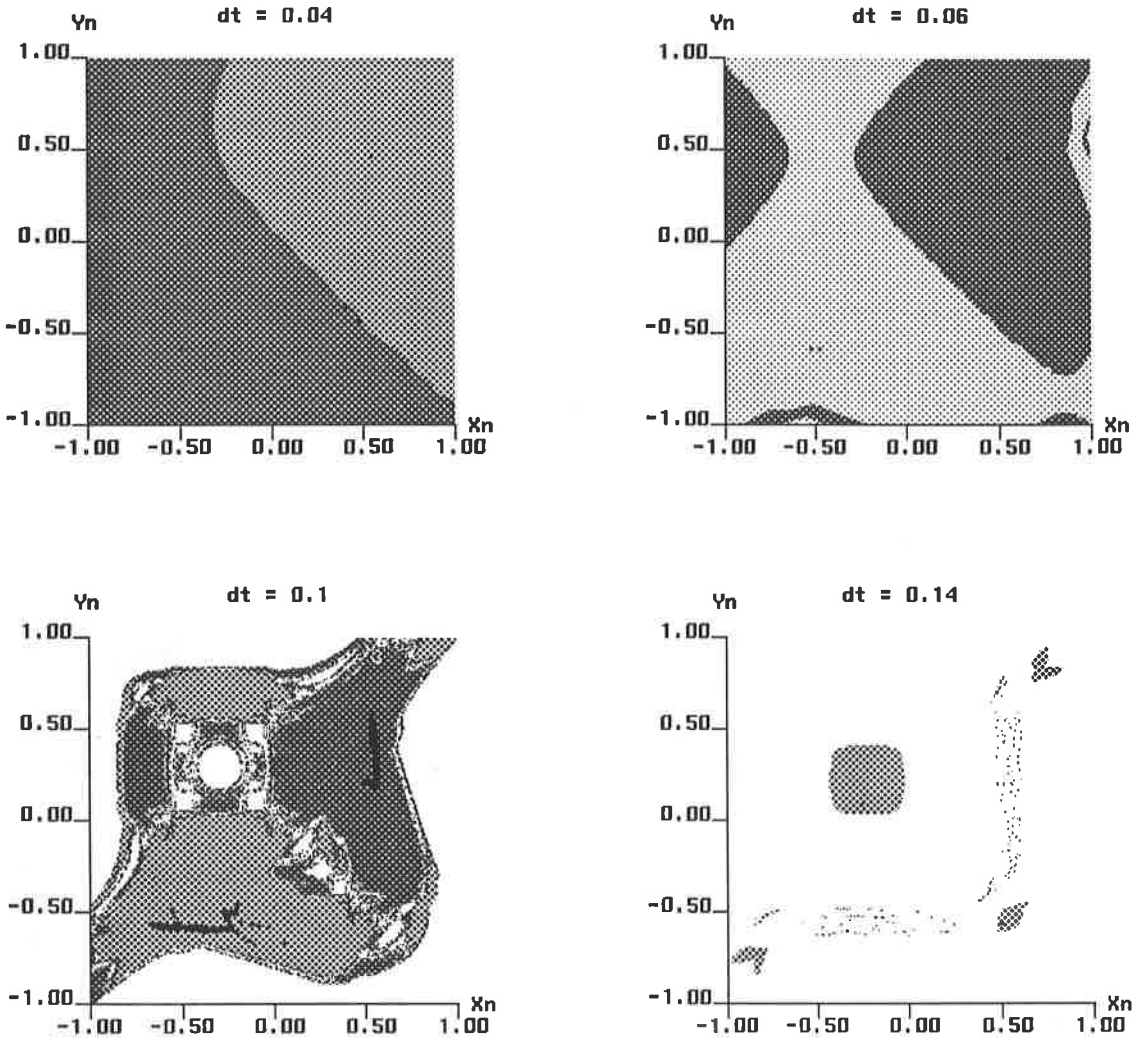

Figure 4.1.20 : Basins for fixed points at the unstable shock. Explicit superbee TVD scheme.

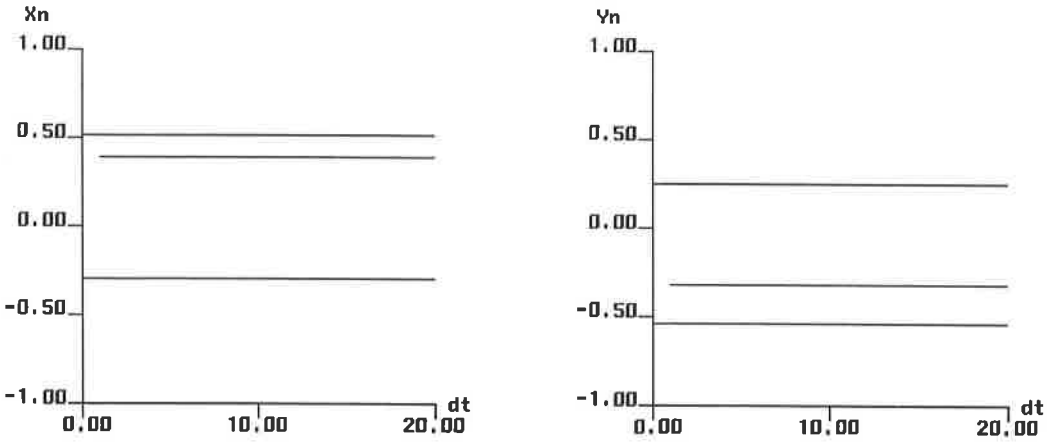

Figure 4.2.1 : Bifurcation diagrams for fixed points at the unstable shock. 1st order implicit E-O scheme.

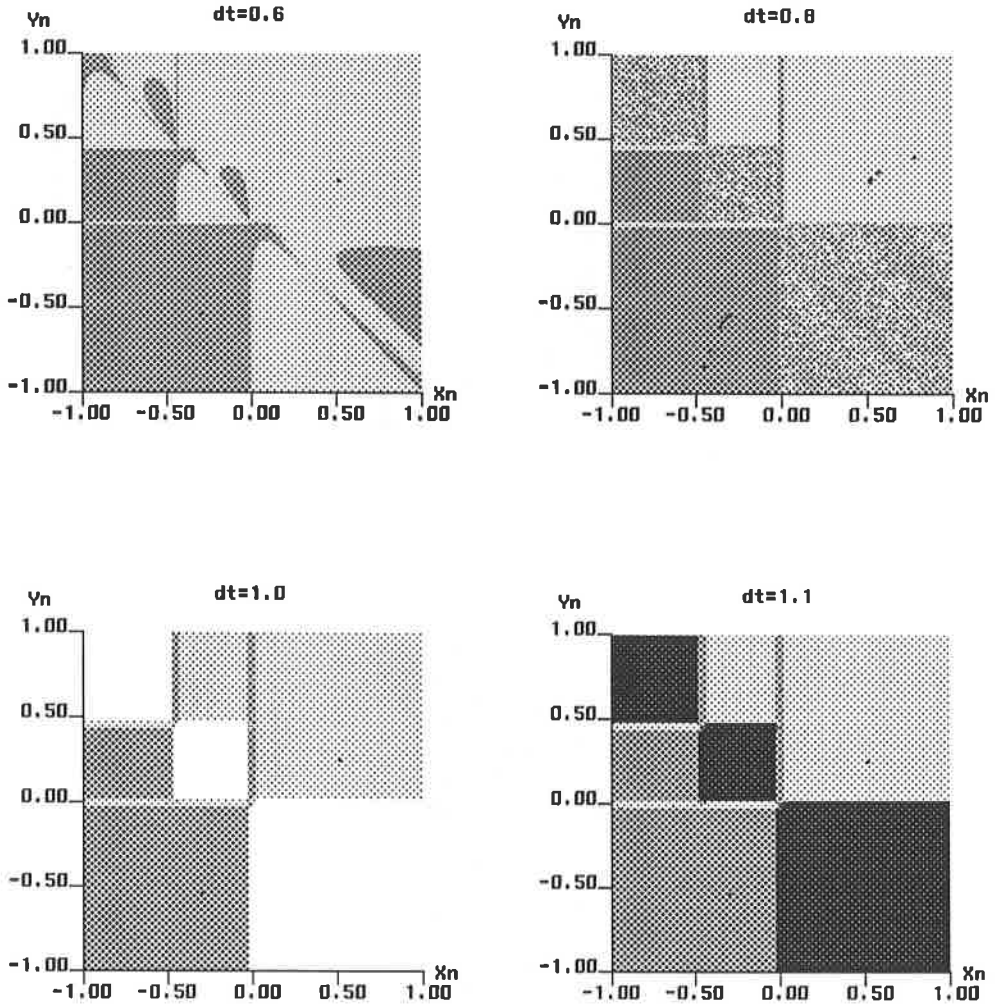

Figure 4.2.2 : Basins for fixed points at the unstable shock. Implicit E-O scheme.

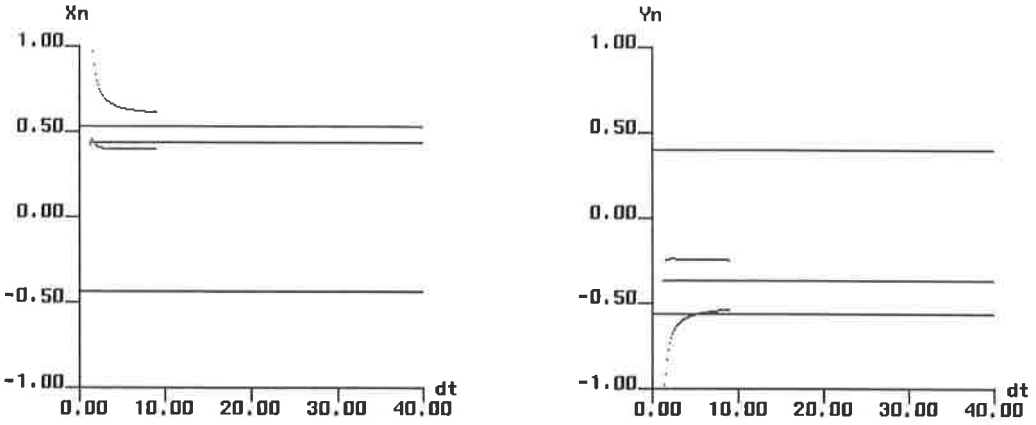

Figure 4.2.3 : Bifurcation diagrams for fixed points at the unstable shock. Implicit minmod TVD scheme.

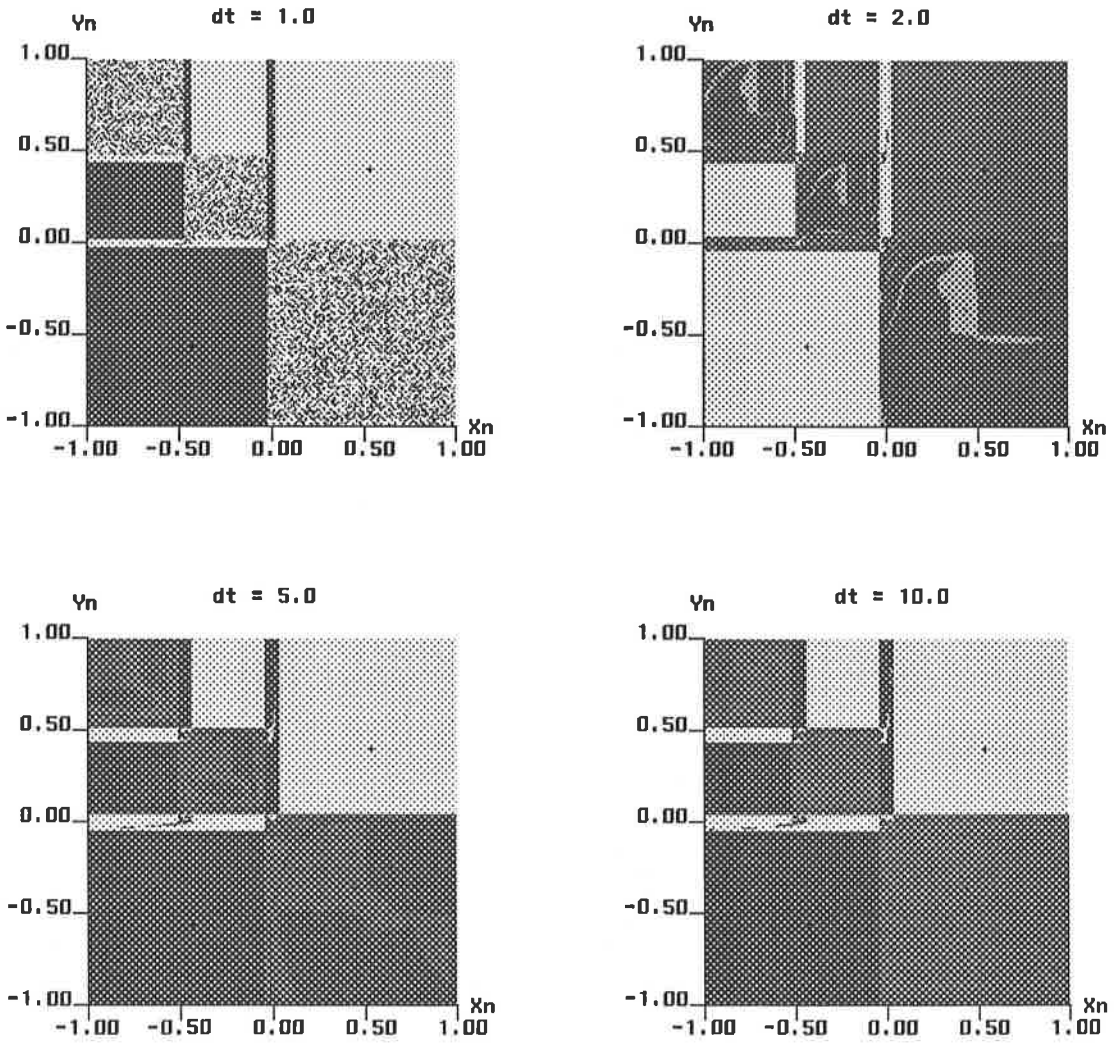

Figure 4.2.4 : Basins for fixed points at the unstable shock. Implicit minmod TVD scheme.

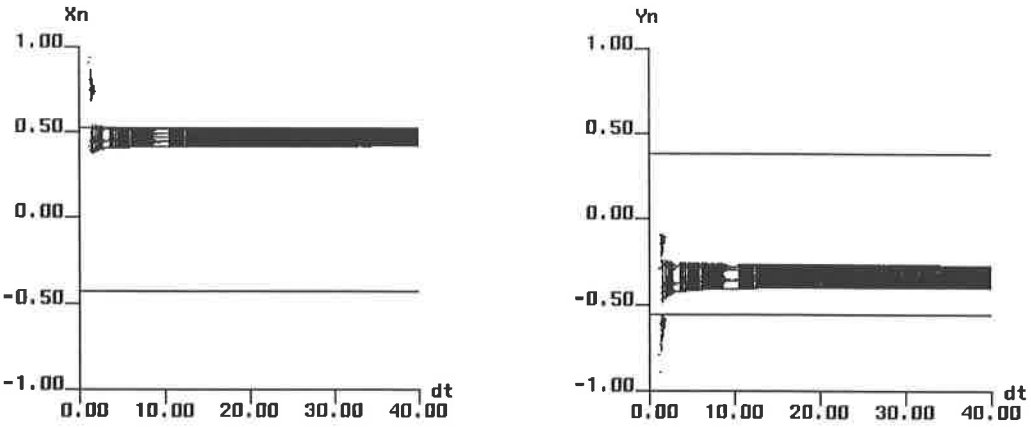

Figure 4.2.5 : Bifurcation diagrams for fixed points at the unstable shock. Implicit van Albada TVD scheme.

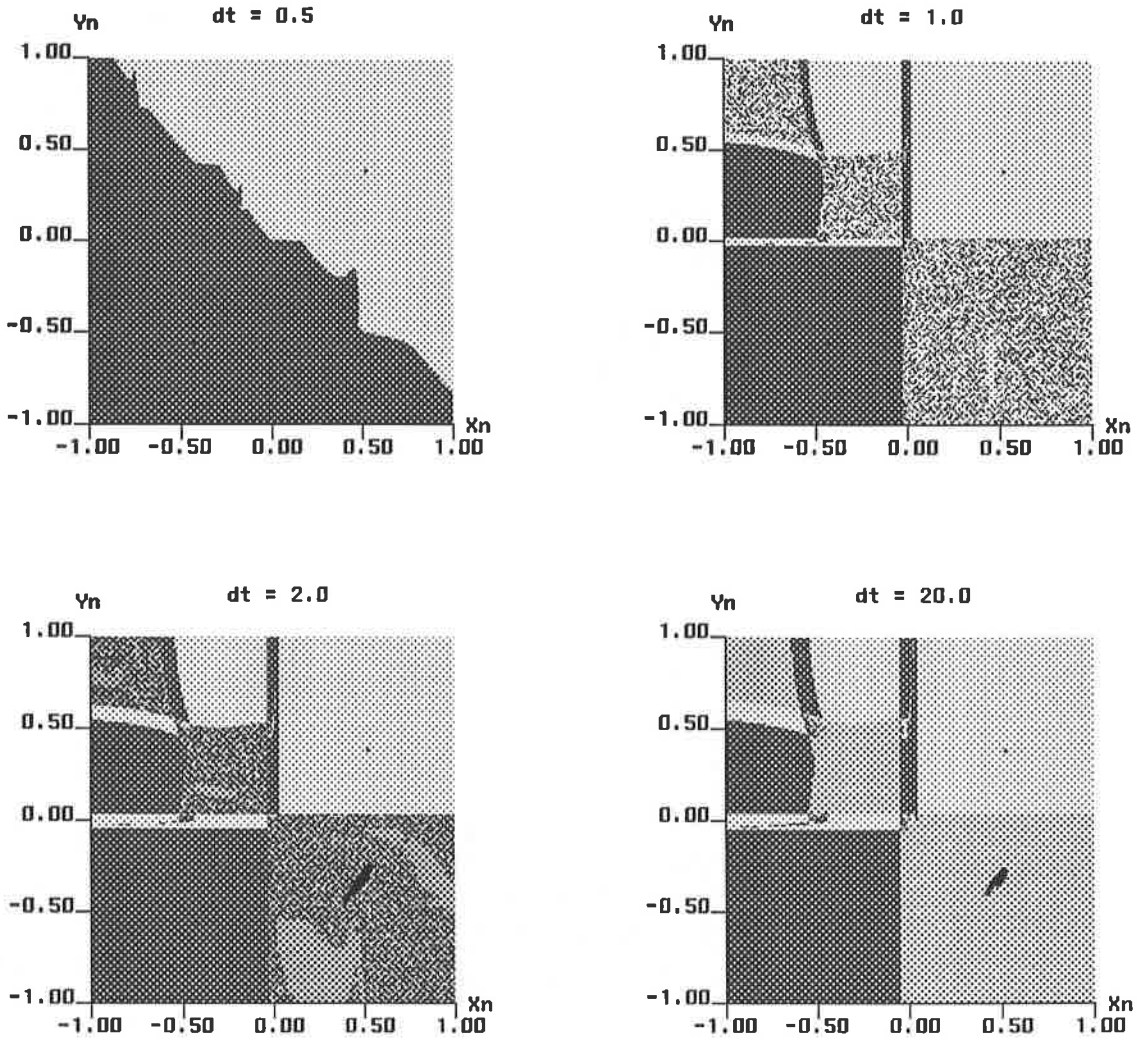

Figure 4.2.6 : Basins for fixed points at the unstable shock. Implicit van Albada TVD scheme.

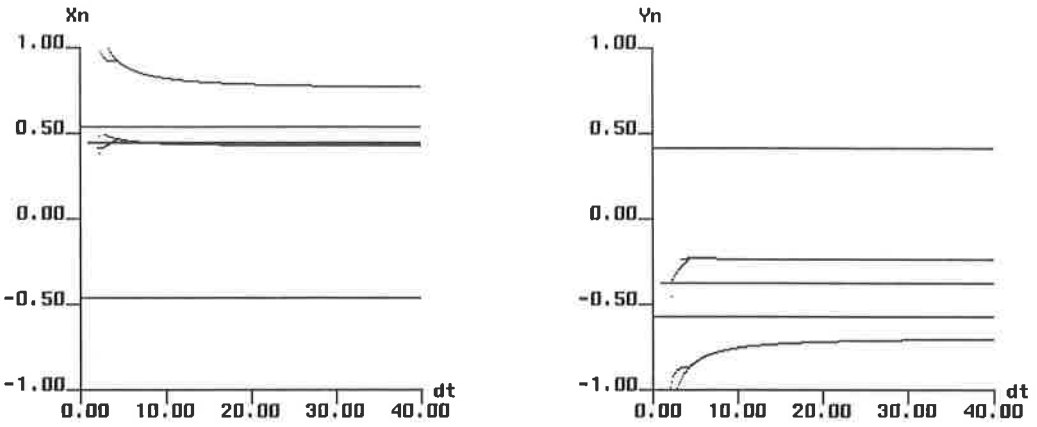

Figure 4.2.7 : Bifurcation diagrams for fixed points at the unstable shock. Implicit van Leer TVD scheme.

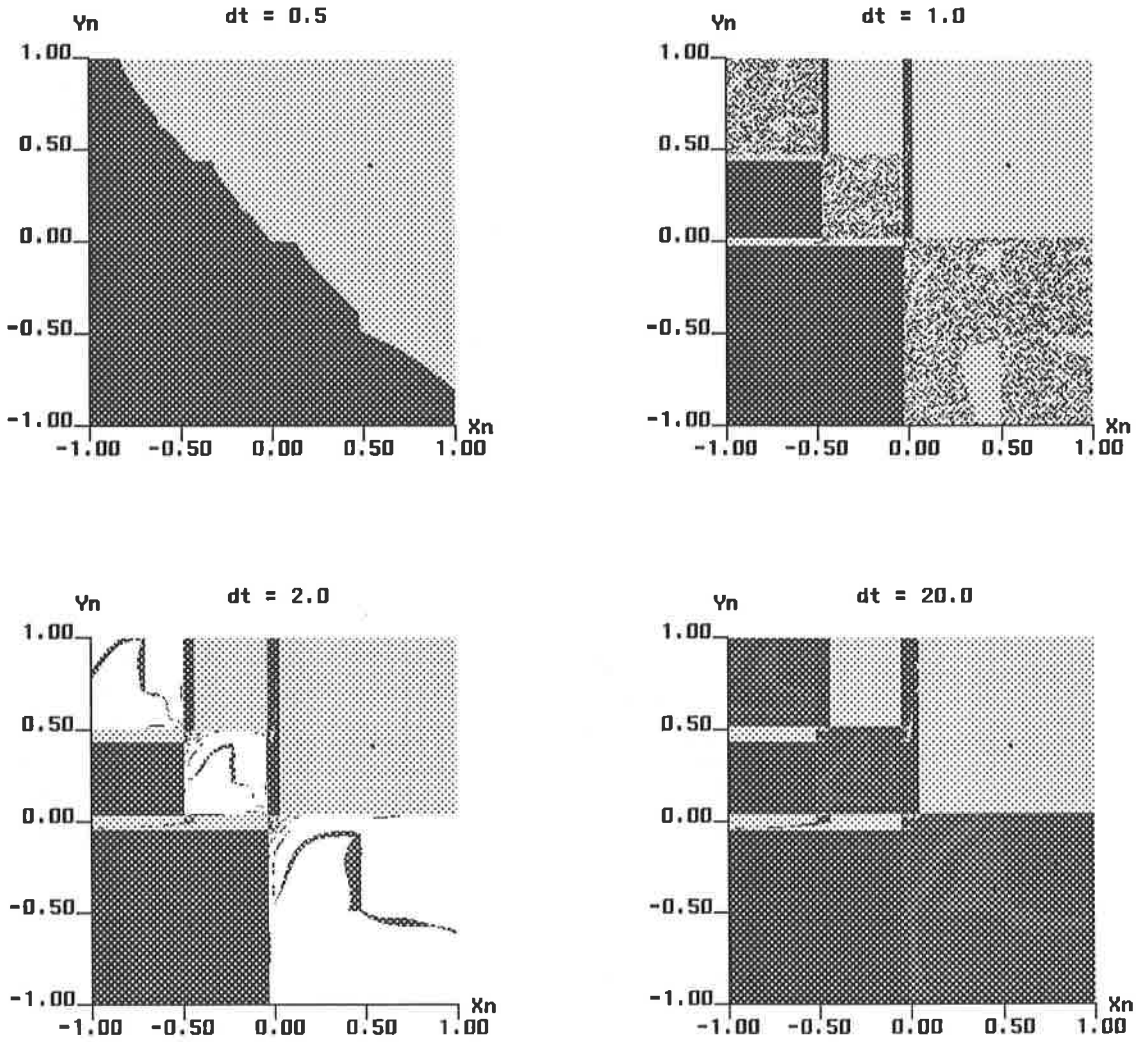

Figure 4.2.8 : Basins for fixed points at the unstable shock. Implicit van Leer TVD scheme.

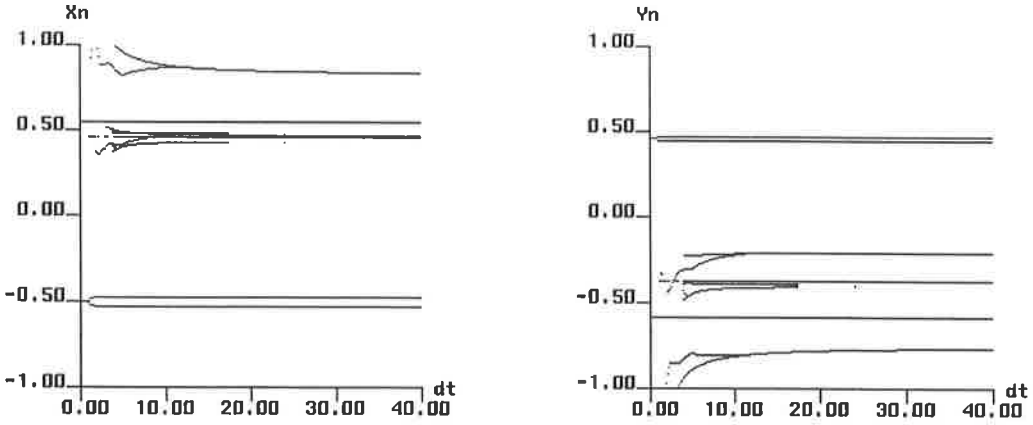

Figure 4.2.9 : Bifurcation diagrams for fixed points at the unstable shock. Implicit superbee TVD scheme.

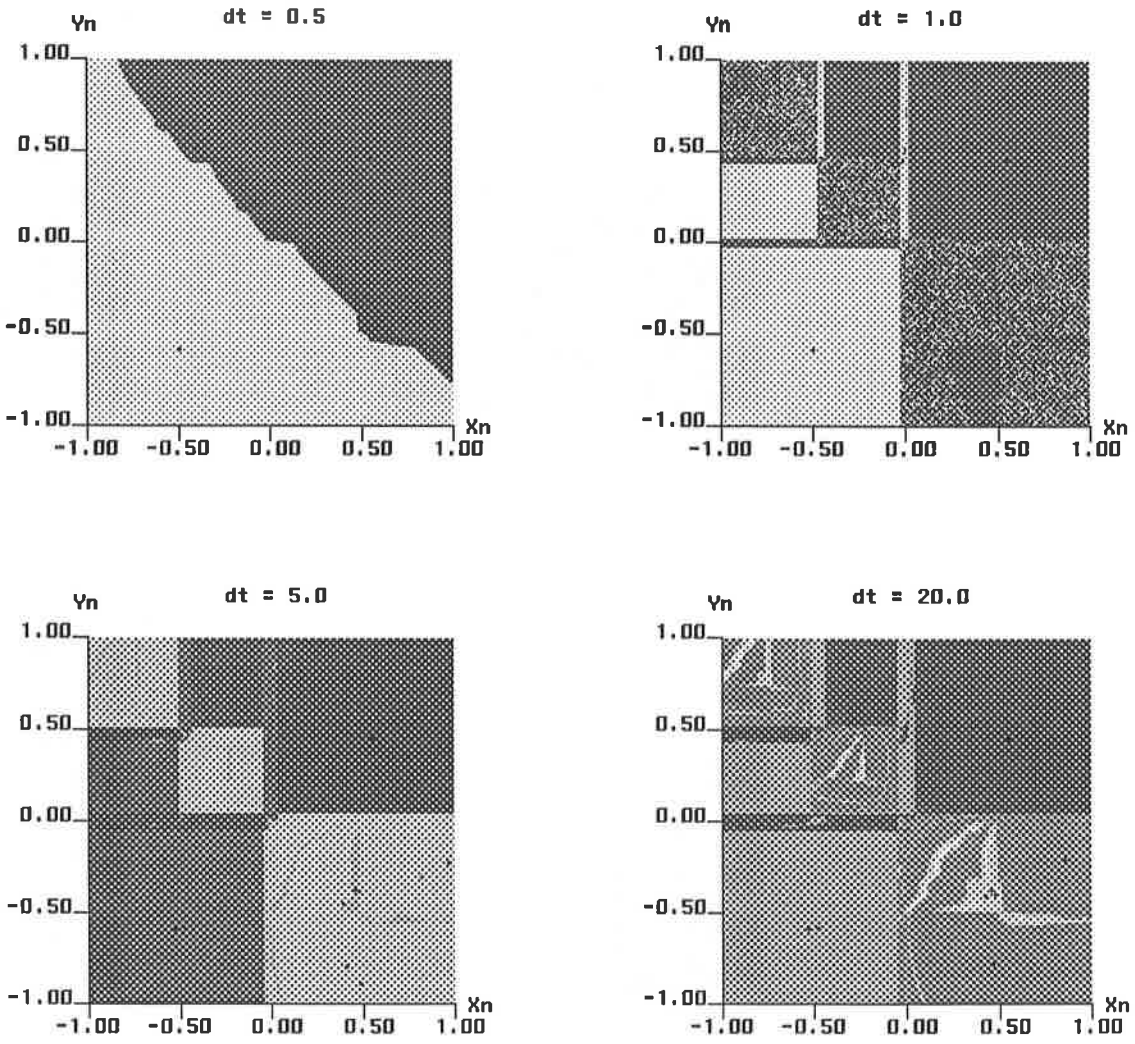

Figure 4.2.10 : Basins for fixed points at the unstable shock. Implicit superbee TVD scheme.

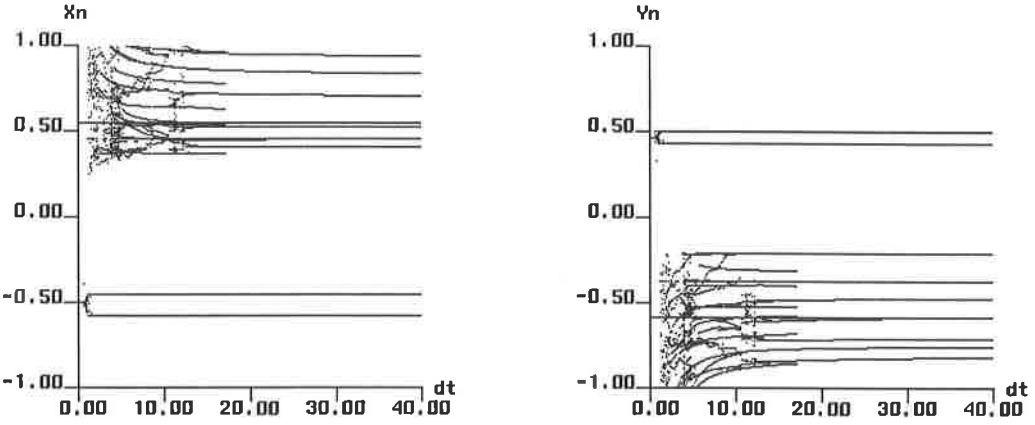

Figure 5.2.1 : Bifurcation diagrams for fixed points at the unstable shock. Implicit superbee TVD scheme with limiter freezing.

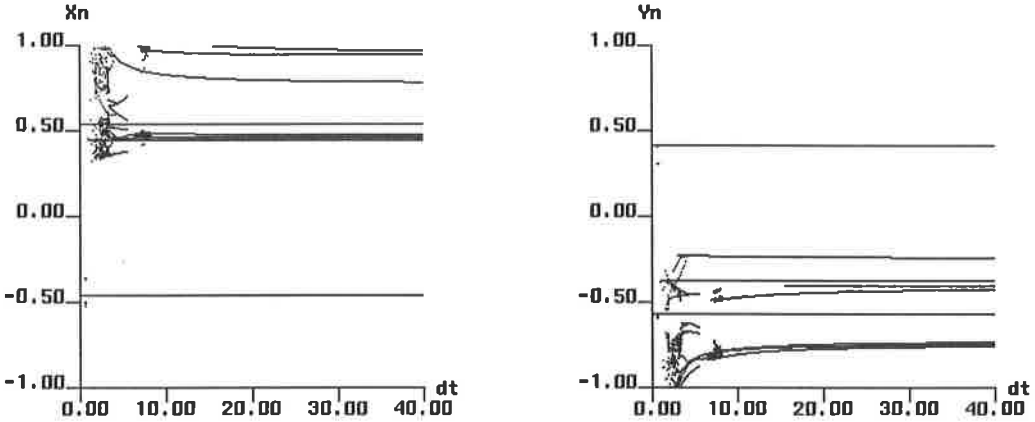

Figure 5.2.2 : Bifurcation diagrams for fixed points at the unstable shock. Implicit van Leer TVD scheme with limiter freezing.

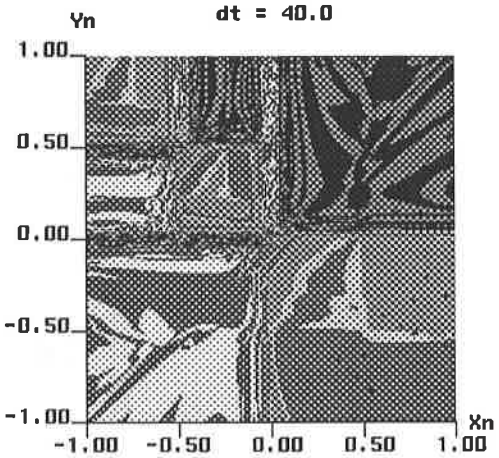

Figure 5.2.3 : frozen superbee

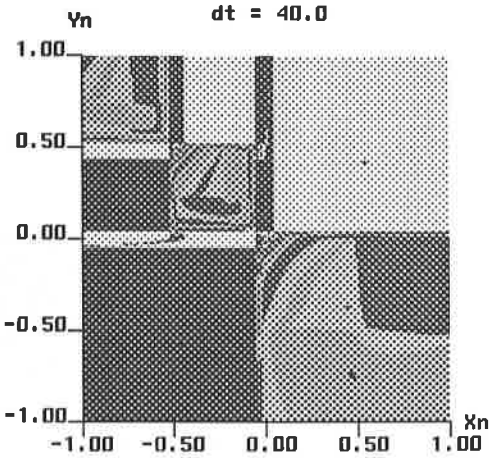

Figure 5.2.4 : frozen van Leer

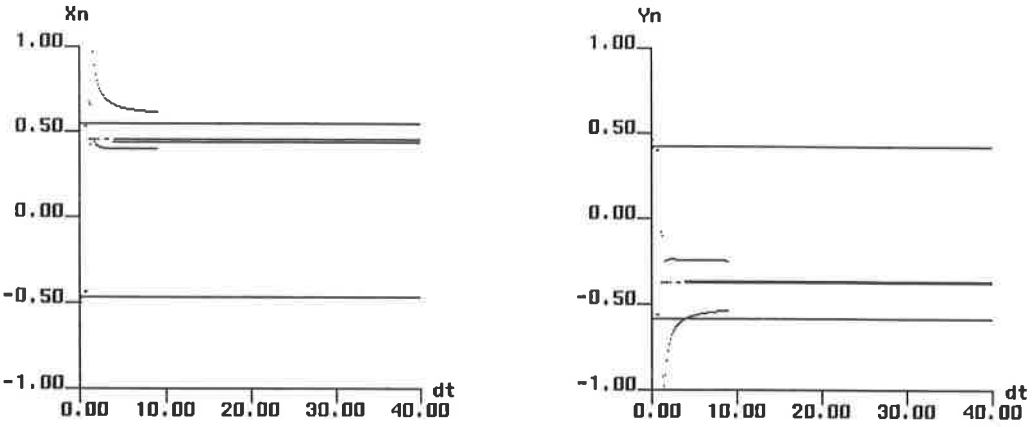

Figure 5.3.1 : Bifurcation diagrams for fixed points at the unstable shock. Implicit superbee/minmod limiter-switching TVD scheme.

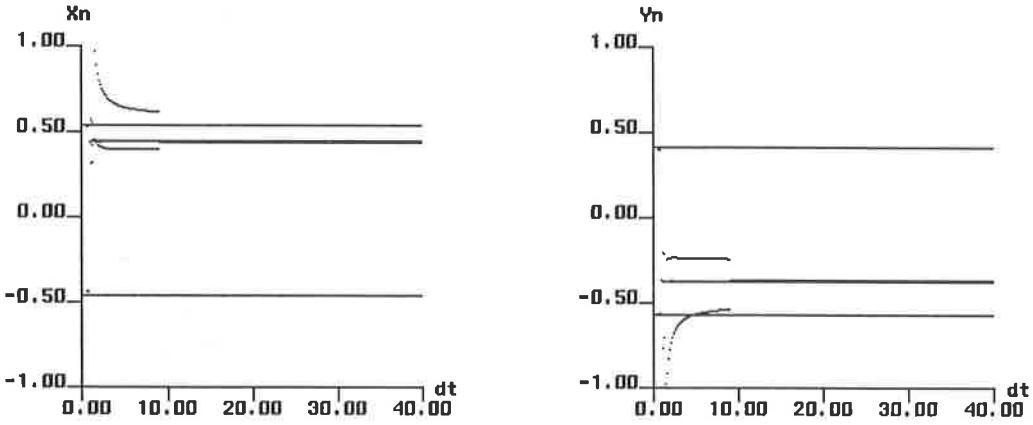

Figure 5.3.2 : Bifurcation diagrams for fixed points at the unstable shock. Implicit superbee/van Albada limiter-switching TVD scheme.

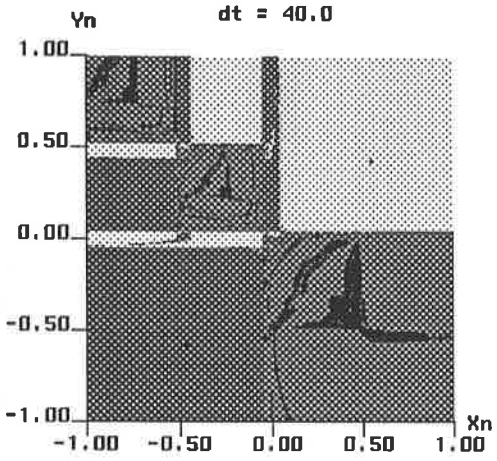

Figure 5.3.3 : superbee/minmod

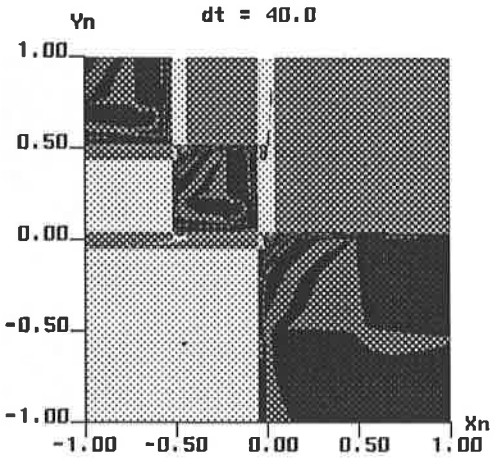

Figure 5.3.4 : van Leer/minmod